JGR Atmospheres

RESEARCH ARTICLE
10.1029/2019JD031255

Drought Demise Attribution Over CONUS

Jiexia Wu[1] and **Paul A. Dirmeyer**[1,2]

[1]Department of Atmospheric, Oceanic, and Earth Sciences, George Mason University, Fairfax, VA, USA, [2]Center for Ocean-Land-Atmosphere Studies, Fairfax, VA, USA

Key Points:
- The transition period leading to drought demise is defined
- A framework for the attribution of several causes of drought demise is devised
- Seasonal variability of drought demise causes is demonstrated

Supporting Information:
- Supporting Information S1

Correspondence to:
J. Wu,
wujiexia0102@163.com

Citation:
Wu, J., & Dirmeyer, P. A. (2020). Drought demise attribution over CONUS. *Journal of Geophysical Research: Atmospheres*, *125*, e2019JD031255. https://doi.org/10.1029/2019JD031255

Received 28 JUN 2019
Accepted 19 JAN 2020
Accepted article online 5 FEB 2020

Abstract Compared with drought onset, the quantification and attribution of drought demise are not well studied. Meteorological droughts usually terminate more rapidly than they initiate, making it hard to define a transition period leading to drought demise with monthly data. In this study, methods of quantifying and attributing drought demise are applied to the Modern-Era Retrospective Analysis for Research and Applications version 2 (MERRA-2) using modified Standardized Precipitation Index representing meteorological drought calculated at pentad intervals to resolve subseasonal demise events. Methodologies to attribute three specific causes of drought demise in nine climate regional divisions over conterminous U.S. (CONUS) are developed. The three phenomenological causes are tropical cyclones, atmospheric rivers, and changes in land atmospheric feedback. Atmospheric river is the most common of the factors for drought demise, over most of the regions in the eastern, and central U.S. tropical cyclones are important causes over the Southwest, the South in fall, and the Southeast in summer. Evolving land atmospheric feedback is a factor mainly over the central and southwestern United States. These attributions estimated may not be representative of the long-term climatologies of drought demise due to the short duration of MERRA-2. A representativeness test is conducted for estimating the three impacts on drought demise using subsamples from a large ensemble of climate model simulation including several centuries of data. Thirty to forty years is not long enough to be representative of local long-term statistics for the attribution of the causes of demise of extreme events like drought but may be adequate at regional scales.

1. Introduction

Droughts are significant environmental disasters that affect agricultural production, regional economies, and society at large (Clark et al., 2002; Marsh, 2007). In the United States since 1980, there have been 25 drought events with an average loss of about 9.5 billion dollars for each event (NIDIS, 2018). Recent observational and modeling studies indicate that an increasing number of drought events are probably related to global climate change (Dai, 2013) and the costs of drought may continue to increase. For example, the 2012 drought in the United States caused about $30 billion in losses to agriculture (Rippey, 2015). According to the U.S. drought monitor (http://droughtmonitor.unl.edu/), 40% of the continental United States had experienced severe to exceptional drought during 2012. Because of the diverse impacts on ecosystems, agriculture, river transport, water supply, and demand, it is difficult to quantify droughts rigorously and consistently (Heim, 2002).

According to the target of their impacts and time-scales, droughts have typically been classified into four categories: meteorological, agricultural, hydrological, and socioeconomic (Dracup et al., 1980; Mishra & Singh, 2010; Wilhite & Glantz, 1985). Recently, a fifth type of drought has been defined: ecological drought (Crausbay et al., 2017). Among these types of drought, there is an order of occurrence. Meteorological drought is caused by lower than normal precipitation over an extended period, and it is the origin of other types of drought. This can trigger agricultural drought, the water shortage in plant-accessible near-surface soil, and how the water deficit impacts crop growth (Mishra & Singh, 2010). As the dryness continues and lateral subsurface water transport slows, the levels of rivers, reservoirs, and lakes decrease (hydrological drought). These three drought types impact different aspects of human activities including industry and domestic water usage, often with political consequences (socioeconomic drought). Ecological drought emphasizes the impact of drought on the natural environment including plant growth, occurrence of wildfires, and wildlife extinction (Crausbay et al., 2017).

Many studies have been conducted to understand the evolution and causes of drought onset (Cook et al., 1988; Fernando et al., 2016; Gommes & Petrassi, 1994; Hoerling & Kumar, 2003; Mo, 2011; Pu et al., 2016;

Seager et al., 2009; Seager et al., 2014; Wood et al., 2015). The main causes of drought onset vary (Mo, 2011; Schubert et al., 2009). Remote oceanic anomalies can alter atmospheric circulations also causing drought. For example, the 1998–2002 drought in the United States, southern Europe, and Southwest Asia were related to cold ocean temperatures in the eastern tropical Pacific and warm temperatures in the western tropical Pacific (Hoerling & Kumar, 2003). Locally, higher than normal surface temperature and high evapotranspiration (ET) paired with a period of reduced precipitation may accelerate drought (Sun et al., 2015).

Compared with drought onset, drought demise has been much less studied (Seneviratne et al., 2006) and is more difficult to estimate because of two main reasons: First, meteorological droughts often terminate rapidly, over the course of days or weeks. Therefore, it is hard to define a transition period leading to drought demise from customary monthly mean data. Drought onset necessarily lasts over an extended period as it results from the accumulated absence of precipitation. Except for flash drought that have a very rapid onset (Christian et al., 2019; Otkin et al., 2019), most droughts build over an extended period, as they result from the accumulated absence of precipitation. In this study, we only study typical droughts with durations longer than 3 months. This period is typically 5–6 months over western United States and can be longer over wet regions in the East (Mo, 2011). Flash drought may occur as fast as termination and daily or pentad based data are needed, but they are not widely used in typical drought events. However, the transition period leading to a drought demise is usually within subseasonal time scales, often lasting less than 2 months (Mo, 2011). Secondly, droughts can terminate for a wide variety of reasons. They can include remote, regional, or local effects, as well as internal atmospheric variability (Xie & Zhang, 2017), which is the unpredictable "noise" arising from nonlinear atmospheric dynamics. We list here three of the major potential causes that operate on subseasonal time scales and discuss how each may contribute to drought demise:

1.1. Land-Falling Tropical Cyclones

TCs are characterized by high winds, coastal storm surge, and extremely intense precipitation that can extend far inland after a TC makes landfall and weakens. TC-related extreme precipitation frequently contributes to drought demise, and the impacts have been discussed using both observed and model data (Kam et al., 2013; Lam et al., 2012; Maxwell et al., 2012; Maxwell et al., 2013; Maxwell et al., 2017; Misra & Bastola, 2016). In the Northeast United States, two thirds of the extremes in precipitation during the hurricane season have been related to TCs (Barlow, 2011), and the affected region from one TC often spans several hundred kilometers. Over the Southeast United States, TCs provide up to 10% of total rainfall amount during the TC season (Knight & Davis, 2007). Therefore, land-falling TCs may play a significant role in drought demise over CONUS, especially in the Southeast United States.

1.2. Atmospheric Rivers

An atmospheric river (AR) is characterized as a plume structure of strong horizontal atmospheric moisture transport with a low-level jet stream, often in advance of a cold front associated with an extratropical cyclone (Ralph et al., 2018). The rate of water mass carried by a typical AR is about twice the flow of the Amazon River. They are recognized as a major reason for extreme precipitation and floods, particularly over the West Coast of the United States (Ralph & Dettinger, 2012). When ARs originating over the Pacific Ocean reach the mountains along the West Coast, the moist air flows upward and creates conditions that favor intense precipitation. In California, about 20–50% of annual precipitation and streamflow is related to ARs (Rutz & Steenburgh, 2012). Due to their intensity and the persistence, ARs can provide beneficial alleviation of droughts (Dettinger, 2013).

ARs also exist over the central and eastern United States and are characterized by moisture flows that come mainly from the south and southeast, originating from the Atlantic, Gulf of Mexico, and the Caribbean (Brubaker et al., 2001; Dirmeyer & Brubaker, 1999; Dirmeyer & Kinter, 2009). From 1963 to 1998, about one third of rainfall over the Mississippi basin in warm seasons originated from local evaporation, while 20% of the rainfall was from the moisture evaporating from Gulf of Mexico and Caribbean (Brubaker et al., 2001). Although less dramatic than the "Pineapple Express" of the U.S. West Coast, ARs over the eastern United States are also a major source of precipitation (Dirmeyer & Kinter, 2009) and a potential contributor to drought demise.

1.3. Land-Atmosphere Feedback

Land atmospheric feedback (LAF) can affect the severity and duration of extreme precipitation events (Hao et al., 2018). However, there is a contradiction in the role of LAF on extremes. On one hand, dry soil produces lower ET, which causes less atmospheric water vapor to be available for precipitation. In dry conditions, near-surface temperatures can increase. This positive feedback mechanism can exacerbate and extend drought (Durre et al., 2000; Fischer et al., 2007; Koster et al., 2009; Mueller & Seneviratne, 2012). Drought demise may occur when this positive LAF is interrupted. On the other hand, over dry soils particularly in dry climates, the high sensible heat fluxes provide buoyant energy that can develop deeper boundary layers and may trigger convection (Eltahir, 1998; Findell & Eltahir, 2003; Roundy et al., 2013; Tawfik & Dirmeyer, 2014). Therefore, in the right conditions, a negative LAF may also increase the chance of rainfall and trigger drought demise.

These three factors are proximate, that is, quantifiable at the location where drought demise occurs. This makes them more direct to diagnose and easier to attribute than remote drivers of drought demise and are thus the starting point for the proposed framework. Previous studies have assessed only single factors of drought demise (Fernando et al., 2016; Ralph & Dettinger, 2012). However, there is a lack of research that compares multiple causes of drought demise. To better understand the major causes of drought demise over the United States, we propose a framework to quantify its period and attribute major potential causes for the demise of each drought. We focus on meteorological over the conterminous U.S. (CONUS) based on precipitation that is available from either observations or model simulations. The study area in this study includes southern Canada, northern Mexico, and part of Caribbean as well as continental United States

We develop and test attribution methodologies using two data sets: the Modern-Era Retrospective Analysis for Research and Applications version 2 (MERRA-2; Gelaro et al., 2017) and the Community Earth System Model, Large Ensemble Project (CESM-LE; Kay et al., 2015). Observations and reanalyses constrained by the assimilation of observations are considered better representations of real conditions but suffer a shortage of data length (Chapman et al., 2015). Thirty to forty is a common period for establishing weather climatologies, anomalies, and extremes from observations and reanalysis. Results from such short durations of data may not represent the climatology of such extreme conditions and their attributions. However, such a short duration of observational data might be suboptimal to represent the climatology of such extreme conditions and to determine their attributions, For this reason, a representativeness test is applied using data from the CESM-LE data set spanning centuries of contemporary climate conditions to determine if the typical data length of observations or reanalysis is adequate to reflect the characteristics of the long-term climatology of drought demise in a relatively stable climate situation. The purposes of the study are (1) to quantify objectively the periods of drought demise, (2) to develop a framework for the attribution of different causes of drought demise, and (3) to evaluate the representativeness of short datasets like those typical of the observational record to long-term estimation of demise statistics. The data sets used to derive droughts and attribute causes of demise are described in section 2. The methods used to identify drought demise, the transition period leading to drought demise, and the attributions of different causes are given in section 3. The attributions of the causes in climate model simulations and the representativeness of short segments of the large model data record are examined in section 4. Conclusions are given in section 5.

2. Data Sets

2.1. Reanalysis and Observed Data

Observationally based assimilated precipitation from the MERRA-2 reanalysis for 1980 to 2015 (Gelaro et al., 2017) is used to identify the transition period leading to meteorological. Five additional observed precipitation data sets are also used to define the meteorological drought and compared with MERRA-2 results to determine the confidence of MERRA-2-based drought demise simulations. They are the Global Precipitation Climatology (GPCP), the Climate Prediction Center Unified Precipitation Analysis (CPC Unified), the Multi-Source Weighted-Ensemble Precipitation (MSWEP), and two versions of the Water and Global Change Forcing Data methodology applied to ERA-Interim data using the bias target Climatic Research Unit (WFDEI-CRU) and the German Weather Service Global Precipitation Climatology Centre WFDEI-GPCC. Table 1 summarizes the details of the six precipitation data sets and provides references

Table 1
Daily Precipitation Data Sets Used to Derive Drought Indices

Product	Spatial resolution	Time period	Source of data
GPCP	1°	1996–2015	Huffman et al. (2001)
CPC Unified	0.5°	1979–2016	Chen et al. (2008)
MSWEP	0.25°	1979–2015	Beck et al. (2017)
WFDEI-CRU	0.5°	1980–2015	Weedon et al. (2014)
WFDEI-GPCC	0.5°	1980–2015	Weedon et al. (2014)
MERRA-2	0.625×0.5°	1980–2015	Ronald et al. (2017)

Abbreviations: CPC Unified: Climate Prediction Center Unified Precipitation Analysis; GPCC: Global Precipitation Climatology Centre; GPCP: Global Precipitation Climatology Project; MERRA-2: Modern-Era Retrospective Analysis for Research and Applications version 2; MSWEP: Multi-Source Weighted-Ensemble Precipitation; WFDEI-CRU: Water and Global Change Forcing Data methodology applied to ERA-Interim data using the bias target Climatic Research Unit.

for each. Below we briefly describe each, as well as the data set used for observed TCs in the vicinity of CONUS.

2.1.1. GPCP

The GPCP One-Degree Daily (1DD) data Version 1.2 are produced by combining the information from the Threshold-Matched Precipitation Index (TMPI) from 40°N to 40°S; elsewhere, the Television and Infrared Observation Satellite Operational Vertical Sounder (TOVS; Susskind et al., 1997) precipitation data and infrared brightness temperature (IR Tb) are used. The data are available from 1996 to present with spatial resolution of 1°.

2.1.2. CPC Unified

The CPC Unified Gauge-Based Analysis of precipitation merges global daily gauge observations and satellite products. About 16,000 quality controlled precipitation stations collected by the National Oceanic and Atmospheric Administration (NOAA) CPC are used, and an optimal interpolation analysis has been applied to the gauged precipitation (Chen et al., 2008). The grid resolution of the data is 0.5°, and the time period used in this study is from 1979 to 2016.

2.1.3. MSWEP

The MSWEP daily global precipitation dataset is produced by weighted averaging from seven precipitation datasets including gauge-based CPC Unified, GPCC, satellite products CPC morphing method (CMORPH), Global Satellite Mapping of Precipitation Moving Vector with Kalman filter (GSMaP-MVK), and Near Real-Time 3-hourly TRMM Multi-Satellite Precipitation Analysis (TMPA 3B42RT), and model reanalysis ERA-Interim and Japanese 55-year Reanalysis (JRA-55). It was developed to be used as a high-quality forcing data set for land surface models including hydrologic and ecological models. High correlations have been found with other independent precipitation data sets such as the GPCP-1DD data and FLUXNET tower stations (Beck et al., 2017; Dirmeyer et al., 2018).

2.1.4. WFDEI

The WFDEI precipitation dataset is a product of EU Water and Global Change (WATCH) project (Harding et al., 2011) based on a combination of observations and the European Centre for Medium-range Weather Forecasts (ECMWF) ERA-Interim reanalysis. WFDEI-CRU and WFDEI-GPCC are the two daily products with two sequential elevation correction and bias correction targets using CRU TS3.1 gridded observations and GPCC (Harris et al., 2014).

2.1.5. MERRA-2

National Aeronautics and Space Administration (NASA)'s Global Modeling and Assimilation Office MERRA-2 reanalysis dataset to replace the original MERRA, featuring improvements to the model parameterizations and the assimilation systems (Molod et al., 2015). One of the major advances of MERRA-2 from the first generation is that MERRA-2 uses observational precipitation data over the land surface as was merged successfully previously into the MERRA-Land product. MERRA-2 precipitation is better than precipitation from MERRA and MERRA-Land because it merges satellite and gauge precipitation data into the analysis (Reichle et al., 2017). Soil moisture at top 10 cm from MERRA-2 is used to identify agricultural drought. The detection, tracking, and analysis of tropical cyclone (TC), AR, and LAF are also using MERRA-2 data. The data information, including the file names and DOIs of the variables used are listed in Table 2:

Table 2
MERRA-2 Data Used to Derive Drought Demise and Three Causes

File name	DOIs	Variables
tavg1_2d_lnd_Nx	10.5067/RKPHT8KC1Y1T	Surface soil moisture (SFMC) Latent heat flux (LHLAND) Sensible heat flux (SHLAND)
tavg1_2d_lfo_Nx	10.5067/L0T5GEG1NYFA	Total precipitation (PRECTOT)

Abbreviation: MERRA-2: Modern-Era Retrospective Analysis for Research and Applications version 2.

2.1.6. HURDAT2

The second generation of the North Atlantic Hurricane Database (HURDAT2) is used to identify the TCs that may affect drought demise over CONUS during 1980 to 2015. HURDAT2 was compiled by the National Hurricane Center (Landsea & Franklin, 2013). This analysis provides information on the best-track positions, intensity, central pressure (beginning in 1979), and storm size (beginning in 2004) for the Atlantic and eastern North Pacific tropical and subtropical cyclones, with data provided every 6 hr.

2.2. Model Simulation Data

To test the representativeness of 30- to 40-year climatologies, CESM-LE (Kay et al., 2015) output are used. The CESM-LE simulations are based on CESM1 with the Community Atmosphere Model Version 5.2 (Hurrell et al., 2013). The main components of the coupled model include atmosphere, ocean (Parallel Ocean Program, version2 [POP 2]), land (Community Land Model, version 4 (CLM 4; Lawrence et al., 2011)), and sea ice (Los Alamos Sea Ice Model (CICE; Kay et al., 2015).

The CESM-LE includes 42 ensemble members (35 prepared by National Center for Atmospheric Research (NCAR) and 7 prepared by the University of Toronto) with simulations spanning 1920 to 2100, and each ensemble member shares the same external forcings. Because of the large ensemble size, many centuries of contemporary climate estimates are available, leading to a more robust estimation of infrequent extreme events such as drought and the factors that contribute to drought demise. However, we limit the data used in two ways. First, for investigating the climatology of drought onset, demise, and transition times, precipitation and moisture in the top 10 cm of the soil column from daily CESM-LE output from 1980 to 2015 (1554 total years across 42 ensemble members) are used, to be consistent with the modern period of observations. For demise attribution, a finer temporal resolution than daily is required to identify the tracks of model proxies of TCs. The 6-hourly CESM-LE data sets are used. Due to the limited length of the 6-hourly CESM data, the time period used to develop the methodology for the attribution of the causes is limited to 1990 to 2005 (672 years in total).

The original spatial resolution of CESM-LE is 1.25°×0.9°, and the output has been regridded for this study to a regular 1°×1° grid for separate comparison to observational data sets not presented here. Daily precipitation is used to derive drought indices. Six-hourly data of wind speed at 850 hPa, surface pressure, and temperature at 300, 500, and 700 hPa are used for TC detection and tracking. Six-hourly wind speed and humidity between 1,000 and 300 hPa are averaged to daily to detect AR features.

3. Drought Demise Definition and Causes

3.1. Transition Period to Drought Demise

Transition periods of drought demise are defined focusing on local severity and local definitions of drought, neglecting aspects of spatial extent often used to characterize major events of severe economic and ecological impact. Among the few studies that have quantified drought termination, Bonsal et al. (2011) identified drought demise for specific events based on spatial extent, when the affected area under severe drought falls to less than 10%. Such an approach is not applicable for a local focus. Margulis et al. (2016) analyzed 2015 drought over Sierra Nevada (USA) using snowpack deficit and estimated drought recovery by applying snow water equivalent to a Monte Carlo analysis (Margulis et al., 2016); Parry et al. (2016) defined the transition period locally from the time of driest conditions to the time that conditions cross back above normal. Since the time between peak dry conditions and the precipitation events that break a drought may be highly variable, the definition may include extensive periods of actual drought where no demise factors are at work.

In this study, we focus on the events that break a drought near the time of return to near-normal conditions and attempt to identify and attribute the processes that cause its demise. Mo (2011) determined the transition period of drought demise by counting the number of positive monthly precipitation anomalies starting 6 months before full recovery. An approach that can be applied to higher frequency precipitation data using robust metrics and appropriate aspects of these methods to enable characterization of causes of more rapid drought demise is needed.

One of the most commonly used meteorological drought metrics is the Standardized Precipitation Index (SPI; McKee et al., 1993), which uses local monthly mean precipitation data to indicate the probability of precipitation total for different time periods, typically from 3 months (SPI-3, short term) to 48 months (SPI-48, long term), estimated at monthly intervals. While this works well for characterizing drought onset and duration, the transition period leading to drought demise is usually no more than one to two months (Mo, 2011). To capture subseasonal drought demise transition periods, a finer temporal resolution data set is required. In this study, we use precipitation totals at pentad (5-day) intervals rather than monthly. For our application, daily data are averaged to pentads (5-day means); a 6-pentad SPI (SPI-6P) at pentad t is computed based on

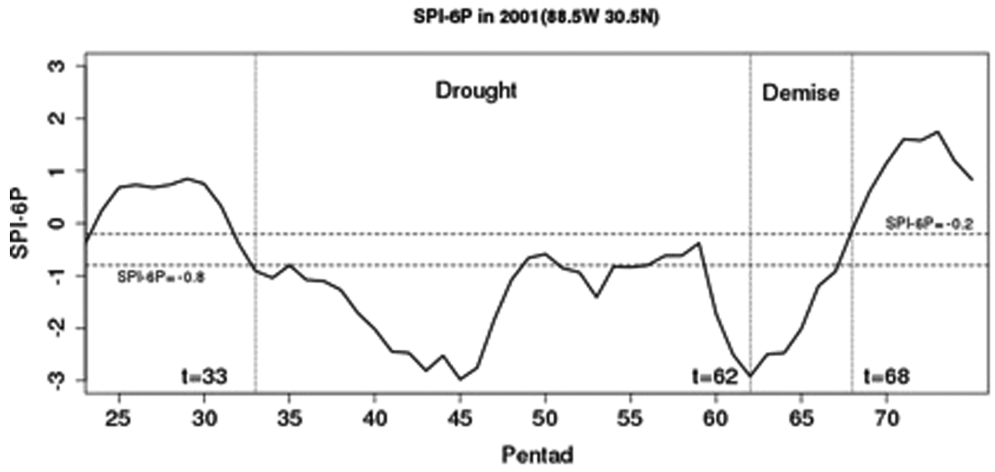

Figure 1. An example demonstrating quantitative identification of a drought demise period.

averaged precipitation anomalies from pentads t–5 to t, effectively 30 days, in a moving window every 5 days. The spatial filter used here is bilinear interpolation.

Meteorological drought onset in this study is defined as a SPI-6P value dropping lower than −0.8, and the drought demise threshold is a SPI-6P rising above −0.2, following Mo (2011). Only those events lasting at least 18 pentads (approximately 3 months) are analyzed. Because pentad-means of precipitation produce noisier time series than monthly data, a new stepwise method is proposed to identify the transition period leading to drought demise. As shown in the example in Figure 1, once the pentad of drought recovery (t=68 in this case) is identified, the transition period leading to drought demise is defined by comparing the drought indices at pentads t and t−1; if the SPI-6P is lower at t−1 than at t, then we move one step back and compare t−2 and t−1 until the driest time (t_d) is found (in this example t_d=62). If this pentad is also the driest in the six surrounding pentads (3 pentads before t_d and 2 pentads after it), then the transition period is defined as from t_d to t; if not, then the driest pentad (t_d) among the six surrounding pentads is selected and the process is repeated (comparing t_d and t_d−1) until the lowest value is identified. This definition of a starting point for demise is similar to the method of Parry et al. (2016) except this could be a local minimum and not the driest conditions for the entire drought period (t=45 in this case).

3.2. Causes of Drought Demise

In this study, we diagnose and attribute the causes of drought demise by location and season over CONUS based on contemporaneous collocated factors; three are examined in this study. To save computational resources as described below, the 6-hourly data used for TC identification and attribution are aggregated to daily to estimate attribution of ARs and LAF without significant loss of accuracy. The specifics of drought demise attribution for each of the three causes are described here.

3.2.1. TCs as Cause

The first potential cause of drought demise assessed is TCs. The drought demise periods at each 1° grid cell are compared with the occurrence and proximity of TCs to establish if they are the likeliest source of precipitation that end drought events. Previous work has shown that the simulated intensities and tracks of cyclones are sensitive to the horizontal resolution of numerical models. For example, the diameters of the TC eyes are typically 10–50 km, which requires a grid spacing considerably finer than 50 km (Fierro et al., 2009; Manganello et al., 2012). To simulate and predict TCs well, a model with a horizontal spatial resolution of less than 10 km is preferred (Manganello et al., 2012). Due to the limitation of the horizontal resolution of MERRA-2,which does produce TC-like warm-core circulation features with similar behavior, the thresholds selected to declare a TC in the model are not as strong as those used for observations and other high resolution models simulations (Walsh et al., 2007). The criteria listed in Table 3 are used.

To identify the TC center, the local minimum of the surface pressure below 1,020 hPa with vorticity exceeding the threshold is selected. A 5° × 5° box centered on the selected point is chosen to define the warm core temperature anomaly, which is the temperature difference of the center point and the average of the rest of

Table 3
Detection Criteria for Tropical Cyclones From MERRA-2.

Location	Minimum surface pressure (hPa)	Vorticity (s^{-1})	Warm core temperature anomaly (K) (T700+T500+T300)	Maximum Wind speed at 850 hPa (m/s)	Latitude	Duration (days)
Initial	1020	2.5×10^{-5}	>0	15	<30°N, ocean	≥2
Ocean	1020	2.5×10^{-5}	>0	10	any	
Land	1020	2.5×10^{-5}	>0	10	any	

Abbreviation: MERRA-2: Modern-Era Retrospective Analysis for Research and Applications version 2.

the grid points within the box. The maximum wind speed is the highest wind speed at 850hPa in the 5° × 5° box. Elevated land areas with annual mean surface pressure lower than 900 hPa are not considered as TC affected areas. Once a grid point meets all the criteria in Table 3, a 5° × 5° box centered on this point is defined to determine if a TC center can be identified within the box at the next time step. After tracking all possible TC events, only the TCs that last at least 2 days (eight 6-hr intervals) while exceeding the criteria in Table 3 are retained for analysis.

The frequencies of TCs per decade based on HURDAT2 and MERRA-2 from 1980 to 2015 are shown in Figure S1 in the supporting information. The spatial distributions of TC occurrences based on the two data sets are quite similar. The active seasons for TC are summer and fall, and the affected areas are mainly over the Southeast United States. The land-falling TCs affecting occur about once per decade in summer and fall in that area. The frequencies of land-falling TC in the Atlantic are much higher than that in Pacific. The land-falling TCs from the Pacific only affect the western coastal areas of Mexico (Table 4).

Although the frequencies of TC based on our detection criteria are underestimated over the tropics, the general pattern over the land is closer to HURDAT2 than over the ocean. Generally, the TC frequencies from MERRA-2 and HURDAT2 show a similar spatial pattern over land. To estimate the impact of TC on drought demise, the following computations for MERRA-2 are based on observational HURDAT2 data, which provide the locations of TC centers. The same TC detection and tracking method has been applied to CESM-LE for the representativeness test, discussed later.

Table 4
The Most Important Factors for Drought Demise and Their Contributions in MERRA-2

	Northwest	West	Southwest	West North Central	South
MAM	AR	AR	AR	AR	AR
	3.5%	1.0%	8.2%	4.3%	40.8%
JJA	AR	AR	LA	AR	AR
	1.5%	5.4%	1.2%	14.5%	18.9%
SON	AR	AR	TC	AR	TC
	4.7%	6.8%	7.1%	9.3%	30.2%
DJF	AR	AR	AR	AR	AR
	22.9%	18.4%	2.8%	4.1%	22.7%
	East North Central	Central	Southeast	Northeast	U.S.
MAM	AR	AR	AR	AR	AR
	26.1%	19.3%	54.8%	46.0%	24.0%
JJA	AR	AR	TC	AR	AR
	57.6%	47.4%	33.8%	62.7%	21.0%
SON	AR	AR	AR	AR	AR
	42.7%	49.7%	39%	45.0%	23.7%
DJF	AR	AR	AR	AR	AR
	12.8%	46.7%	57.5%	43.7%	24.1%

Abbreviations: AR: atmospheric river; DJF: December-January-February; JJA: June-July-August; MAM: March-April-May; MERRA-2: Modern-Era Retrospective Analysis for Research and Applications version 2; SON: September-October-November; TC: tropical cyclone.

After identifying all TC positions in each ensemble member of the MERRA-2, the established dates and locations of MERRA-2 drought demise are compared with the TC events. According to Barlow (2011), 500 km is the average impact radius for a TC. Thus, MERRA-2-based precipitation within a 5° radius from the center of the TC is considered to be attributable to the TC. If during the demise period a TC center is present within 5°, then TC will be identified as a contributing cause to the drought demise.

The attribution of TCs and TC-related precipitation to drought demise are quantified in two ways. The first is the ratio of the number of drought demises related to TCs to the total number of drought events r_1.

$$r_1 = \frac{\text{Nr of drought demise related to TC}}{\text{Total Nr of drought events}} \tag{3.1}$$

This gives a count of the fraction of droughts whose demises are likely influenced by TCs. Secondly, the ratio of total TC-related precipitation (SPI-6P change) to the total precipitation deficit (SPI-6P deficit) is estimated:

$$r_2 = \frac{\text{SPI}-6\text{P change related to TC}}{\text{SPI}-6\text{P deficit}} \tag{3.2}$$

r_2 shows the fractional contribution of TC related precipitation toward drought demise totaled over all relevant events, whereas r_1 weights all

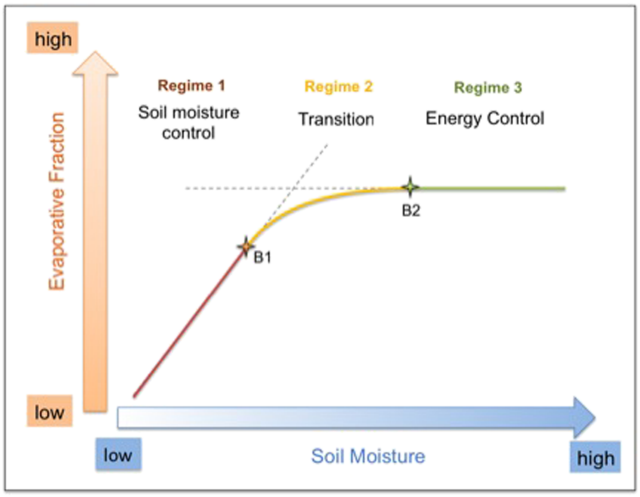

Figure 2. Diagram relating evaporative fraction and soil moisture wherein three regimes are defined based on Koster et al. (2009).

contributing TCs equally regardless of how much precipitation occurs. If the precipitation of any pentad is identified as associated with a TC, this pentad will no longer be considered in the following time steps.

3.2.2. ARs as Cause

The second potential cause to identify is ARs. The AR data are computed based on MERRA-2 by following the method of (Mundhenk et al., 2016). ARs are identified by the magnitude of integrated water vapor transport, which is calculated by vertically integrating the horizontal moisture transport between 1,000 and 300 hPa. An anomalous integrated water vapor transport of 250 kg $\cdot$ m^{-1} $\cdot$ s^{-1} is used as the threshold to detect AR features. If a target feature contains more than 100 contiguous grid cells, this feature will be considered as potential AR feature. The ratio of major axis length to minor axis length historically used to detect AR features is at least 1.6:1. Unlike TCs, the identified ARs are large-scale features with at least 100 contiguous grid cells at 1° resolution. The daily AR calculations are first compared with the model precipitation locally; the precipitation is identified as AR-related if there are positive precipitation anomalies at the locations where an AR event occurs. In that case an AR is considered as a potential cause for drought demise. The transition period of drought demise is identified and compared to the dates with ARs that extend over land. The two methods to calculate the ratios of ARs related drought demise to the total number of droughts are the same as for TCs.

3.2.3. LAF as Cause

LAF regimes are identified according to the relationship between soil moisture and evaporative fraction (EF), which is the ratio of latent heat to the sum of latent heat and sensible heat. Figure 2 shows the idealized relationship between EF and soil moisture based on Koster et al. (2009). In Regime 1, surface fluxes are strongly controlled by soil moisture. In this regime, soil moisture and EF are positively correlated (slope $>$ 0) and LAF is in effect. For this regime, soil moisture is not sufficient to supply maximum ET (i.e., ET is lower than potential evapotranspiration [PET]). The direct dependency of ET on soil moisture affects atmospheric moisture content and moist static energy, which can affect precipitation as a further positive feedback. Thus, drought may be extended or amplified by positive feedback between the atmosphere and dry soil. Regime 3 is the regime of energy control of surface fluxes. For this regime, soil moisture is sufficient that ET can approach PET. Limitations from net radiation, rather than water availability, determine evaporation rates. Here EF is not sensitive to soil moisture variations and no positive feedback from the land surface is realized (slope $\cong$ 0). Regime 2 is a transitional regime between soil moisture control and energy control where LAF strength could change with small soil moisture variations.

In drought conditions, when the soil moisture is lower than the transition regime (soil moisture lower than B1 in Figure 2), positive feedback can support dry conditions. However, if the soil moisture becomes higher than the values in the transition regime (soil moisture higher than B2 in Figure 2), the positive feedback ends and may facilitate drought demise. The actual relationship between EF and soil moisture, and the transition points (B1 and B2), may also vary with other environmental conditions (Haghighi et al., 2018). For example, PET may be lower in fall than in summer at the same location. Or, the same soil moisture level may be sufficient to maximize EF in fall but not summer. In this case, summer is in Regime 1 or Regime 2, while fall is in Regime 3. The positive relationship is removed due to the seasonal change of LAF, and it may relate to drought demise. In this study, we consider only the existence of a mean annual cycle of the curve depicted in Figure 2, from January to December as estimated from MERRA-2. In Koster et al. (2009), four types of LAF regimes are defined according to the relationship of soil moisture and EF. The fourth regime, which is not discussed above, is for arid areas falling to the left of Regime 1 in Figure 2. In arid areas, soil moisture can be too small to cause soil moisture variation and evaporation variation compared with other factors. In this study this regime is included as part of Regime 1.

Based on the definitions of these three regimes, positive LAF (Regime 1) helps the drought conditions to continue when soil is dry. Drought demise could happen under two possible situations: (1) Soil moisture

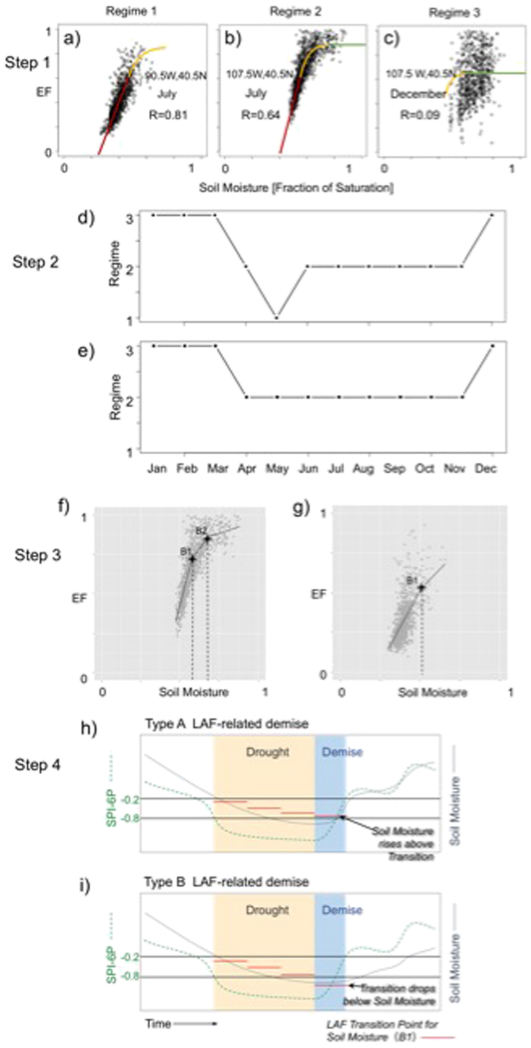

Figure 3. A flowchart of themethodology to estimate the impact of L-A interactions on drought demise. (a)-(c)Examples of the three LAF regimes based on the relationship between EF and SM; (d)-(e) Thecoupling before and after temporal and spatial filters; (f) Segmented regression with two transitionpoints for regime 2; (g) Segmented regression with one transition point for regime 2; (h)-(i) twotypes of LAF impacts on drought demise.

increases beyond the transition regime, thus terminating the positive feedback. (2) The transition regime at a location shifts with the progression of the seasons without an increase in soil moisture. For example, the correlation between EF and soil moisture is positive at a particular value of soil moisture at a location in summer but is near zero in the other three seasons. In this case, the LAF sustaining drought may be removed simply by the progression of the seasons (Dirmeyer et al., 2009). The steps to estimate the impact of LAF on drought demise follow the schematic presented in Figure 2 and are depicted in Figure 3:

1. Defining three LAF regimes

The LAF condition at each grid point for each month from January to December are firstly classified into three regimes according to the relationship between EF and soil moisture based on daily data accumulated from MERRA-2.:

2. Regime 1: *Soil moisture controlled regime*. Figure 3a is an example of Regime 1 for a grid cell at 90.5°W, 40°N for July. The relationship between soil moisture and EF are defined based on daily MERRA-2 output in July from 1980 to 2015. This regime is defined by a correlation between soil moisture and EF higher than 0.8, or for arid areas when the soil moisture value at the 75th percentile as defined locally for the month at that grid cell is less than the soil moisture value defined over CONUS at the 10th percentile in the same month. We select the 75th and 10th percentiles because the spatial distribution of the arid areas is close to Koster et al. (2009).
3. Regime 2: *Transitional regime*. These areas may be some combination of soil moisture controlled and energy-controlled. According to Figure 2, there is a significant slope change in this regime, between B1 and B2. Also, the correlation between soil moisture and EF decreases as soil moisture increases in this regime. In this study, the transitional regimes are defined as areas and months having a correlation between soil moisture and EF lower than 0.8 but higher than 0.5.
4. Regime 3: *Energy controlled regime*. This regime is defined by a correlation between soil moisture and EF less than 0.5, or for wet regions. Wet regions are defined when and where the local soil moisture value at the 25th percentile for the month at that grid cell is less than the soil moisture value defined over CONUS at the 90th percentile in that same month (predominant in Figure 3c).

5. Temporal and spatial filtering

This classification scheme is applied to each grid cell in each of the 12 months, defining a mean seasonal cycle of regimes and transition points B1 and B2 (when they can be defined) for each location. Because of the selection of thresholds in the first step, a jump from one type to another may occur temporally and also vary spatially. Therefore, temporal and spatial filters are applied to the classification (example in Figures 3d and 3e). A moving filter is applied to all the 12 months with a 3-month window. If the first and third months are in the same regime while the second month is not, then the second month is reclassified. Spatially, if the eight connected neighbors of a grid cell are in the same regime while the center grid is not, then LAF regime of the center grid cell is reclassified.

6. Defining B1 for Regime 2

In Figure 2, B1 is the transition point of Regimes 1 and 2. From B1, the positive correlation decreases as soil moisture increases. Therefore, we consider that B1 is the soil moisture level that the positive feedback is removed. To identify B1, we applied a segmented regression (Muggeo, 2003; Muggeo, 2008) to all grid cells

and months that are classified as Regime 2. The segmented regression analysis is conducted by using the package "segmented" in R. As shown in Figure 2 the slope changes gradually around the transition points (B1 and B2), In this study, we first apply a segmented regression with two transition points (B1 and B2 in Figure 3f) to the data to define a transitional range of soil moisture where the LAF change from soil moisture controlled to energy controlled regime. Within this transitional regime (from B1 to B2), the LAF gradually changes from strong to weak or zero as soil moisture increases. The smaller soil moisture value of the two identified transition points (B1) is used as the transition point out of the soil moisture controlled regime.

Due to the different relationships of EF and soil moisture and the initial values of soil moisture provided to find the transition points, it may not always be possible to find two transition points. In that case, we apply segmented regression with one transition point (Figure 3g). For those grid cells that fail to provide any transition point, indicating the relationship between EF and soil moisture does not fit the curve of the transitional regime (Regime 2 in Figure 2), we reclassify them to the energy-controlled regime (Regime 3 in Figure 2).

7. Defining Type A and Type B LAF changes during drought demise

The final step is to relate the LAF regimes and defined transition points to drought demise based on MERRA-2. There are two ways that LAF can be related to drought demise.

1. Type A: In this type of LAF-related demise, the area is in a soil moisture controlled regime with positive LAF (Regime 1 or Regime 2 with low soil moisture) during the drought period, suggesting the dry land surface state is helping maintain drought conditions. The positive LAF terminates with sufficient increase in soil moisture from precipitation (including from TCs or ARs) such that the transition point (B1) is exceeded during the demise period (Figure 3h).
2. Type B: In this type of LAF-related demise, a drought continues through one or more months when the LAF is positive (Regime 1 or Regime 2 with low soil moisture). The drought terminates in a month in which LAF transitions to Regime 3 not due to an increase in soil moisture but due to the evolving seasonal cycle of LAF at that location. The evolution may be a shift downward in the transition threshold (B1 decreases; e.g., Figure 3i), or the complete loss of moisture control on EF, as is often the case in midlatitudes for winter.

This process has been applied to MERRA-2, and the number of drought demise events showing Type A or Type B LAF changes is divided by the total number of drought demise events to estimate their percentage of occurrence.

A flowchart summarizes the steps of this framework in Figure S2. A single drought demise event may be attributable to one or more of the causes listed above. If none of the above correspond to a particular period of drought demise, then we assume that the cause comes from other sources, such as changes in large-scale circulation driven by teleconnections to remote ocean temperature anomalies, precipitation associated with atmospheric baroclinicity (e.g., midlatitude dynamics), or other sources of internal atmospheric variability, which are beyond the scope of this investigation but are discussed briefly in section 5.

3.3. Representativeness Test

We have the general limitation that the time period of the observational record is rather short; 30 years is commonly used to compute many climate normals, and 36 years of MERRA-2 data are used here. Representativeness of the contributions of the three main causes of drought demise is tested in subsamples of the ensembles from CESM-LE against statistics derived from the remaining ensemble members (an out-of-sample test).

The 6-hourly CESM-LE data are from 1990 to 2005 (16 years), with 42 ensemble members in total. Here two to nine of ensemble members having high time-resolution output, spanning 32 to 144 years of data, are selected from the total of 42 ensemble members, and a comparison of estimated statistics is conducted between these subsamples and the remaining ensemble members. A Monte Carlo sampling method is used to select ensemble members, and a comparison between the selected and remaining ensemble members is applied on a grid cell by grid cell basis. If the absolute difference between the ratio of TC (or AR, LAF)-related drought demise based on the selected ensemble members and the ratio of all the ensemble members is lower than 0.05, then we define that the ratio calculated based on the selected ensemble members is representative of the long-term data. If the ratio based on selected ensemble members is 0

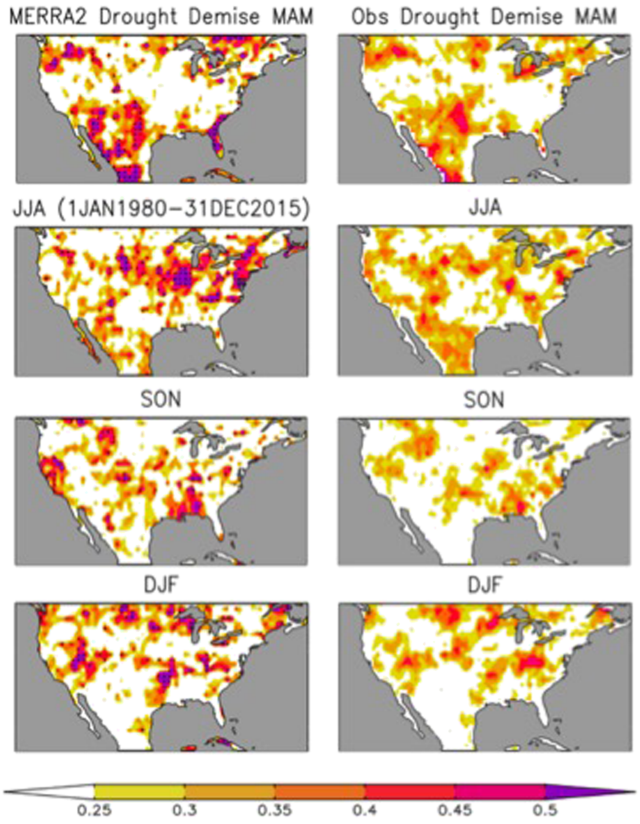

Figure 4. Preferred seasons for drought demise in MERRA-2 and the average of five observations.

(i.e., no events found), then no further comparison is conducted. For each grid cell, the sampling and comparison has been repeated 10,000 times. This results in oversampling for the case of two ensemble members, because the total combinations for two ensemble members are 861 ($_{42}^{2}C = \frac{42!\times(42-1)!}{(42-2)!\times 2!} = 861$). For all other cases, the number of possible combinations exceeds 10,000. If for one grid cell the comparison can be conducted in more than 10% of the selections (i.e., attributable drought demises exist), the percentage of comparisons showing representativeness (difference between −0.05 and 0.05) is calculated, giving a spatial representation of relative representativeness that informs application of this method to the observational record, specifically the recent period typically covered by atmospheric reanalyzes and observational data sets.

Note that there is an implicit assumption of climate stationarity in this approach, as the time period of the historical simulations in CESM-LE is the same 16-year period in each ensemble member (same atmospheric composition, aerosols, etc.). Of course, the current climate is not stationary. However, for purposes of establishing the robustness of using records of a few decades to estimate the likelihood of events that may cause drought demise, this approach is reasonable. The nonstationarity of climate is an additional factor not considered in this study, but the consequences are discussed in the conclusions.

4. Results

4.1. Drought Demise

Figure S3 presents the drought frequency over the United States from MERRA-2. From 1980 to 2015, no more than five drought events are found over the United States in each season. Summer is the preferred season for drought in California, about four cases during this period. About three to four drought cases are observed in the southern United States in winter. Figure 4 shows the preferred seasons for meteorological drought demise based on MERRA-2 and the average of the five observed precipitation datasets. The values show the fractions of drought demise that occur in each season; if equally distributed, the ratio of each season is 0.25. Therefore, only ratios higher than 0.25 are shown. Additionally, only values >0.25 exceeding the 95% confidence level are shown for MERRA-2 data, but there is no screening for the observed multisource precipitation data because the lengths of data sets combined for this estimate are not uniform among products. Although the spatial distribution based on the averaged precipitation data is smoother, the two estimates are similar. Using pentad precipitation data and SPI-6P, spring is the preferred season for drought onset over the central United States. Fall is the preferred season for meteorological drought onset over the northern United States and also the western United States. Droughts in California and parts of the southeastern United States are more likely to occur in summer. The preferred season of drought onset over the Southwest United States and Mexico is winter.

As discussed previously, drought demises estimated from SPI-6P preferably occur about one or two seasons after onsets. Meteorological droughts over the central United States are more likely to end in summer, and the preferred season for drought demise over the northern United States is winter. Drought recovery over the Southwest United States is more likely to occur in spring.

To test if monthly data, most commonly used in previous drought demise studies, would be adequate to capture these drought demise periods, we also compute the average transition period leading to meteorological drought demise (Figure 5). Generally, the transition period is about 3–7 pentads from drought to recovery over all the seasons, in the subseasonal time range. More than 50% of the United States shows that the transition period leading to drought demise is less than 5 pentads, shorter than 1 month. Longer durations (>5 pentads) are found along the western coast of United States in spring and the Southwest United States in

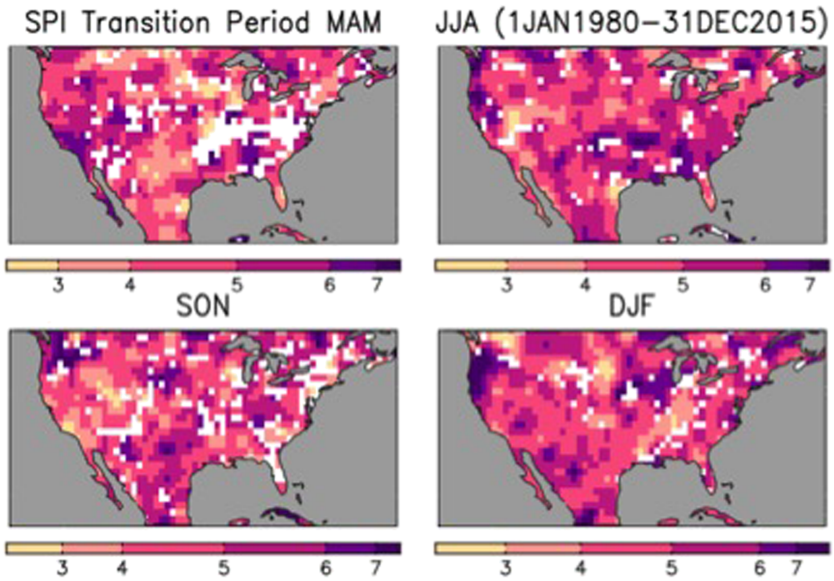

Figure 5. Durations (in pentads) of transition periods leading meteorological drought demise. The length of each band in the color bar is proportional to the fraction of shaded area in each range.

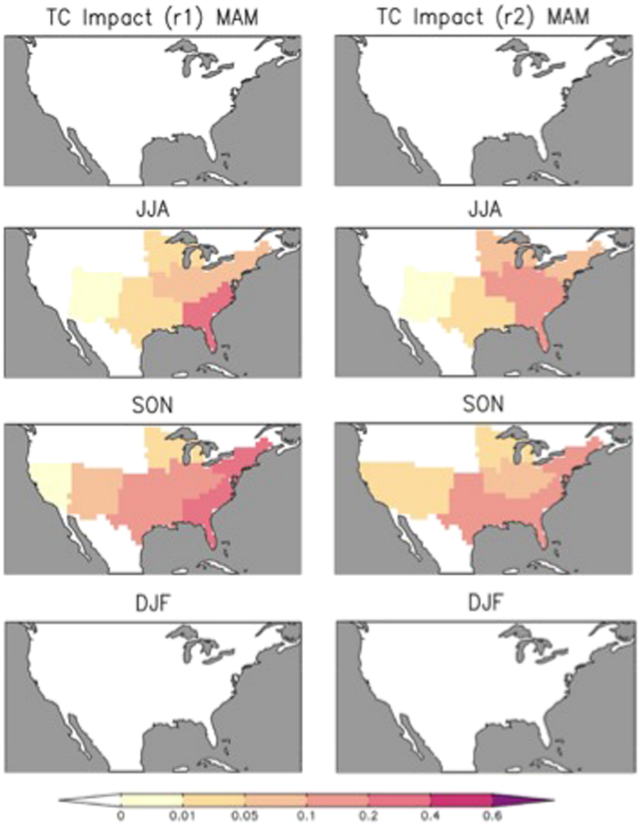

Figure 6. The ratios of tropical cyclones (TCs) occurring during drought demise to the total number of drought events (r1; left four panels); the ratio of TC-related SPI-6P changes to the magnitude of SPI-6P change required to cause drought demise (r2; right four panels) in nine climate regional divisions.

summer. The transition periods are longer than 5 pentads in the Southeast United States in summer. Generally, the transition periods are less than one month (6 pentads) and of course are not likely to align with the start of the months. The results based on MERRA-2 also suggested that when analyzing drought demise, temporal resolution higher than monthly is needed.

4.2. Drought Demise Attributions

Three potential drought demise attributions including TC, AR, and LAF are tested based at MERRA-2 grid cell resolution and also aggregated to nine U.S. regional climate divisions as defined by the CPC, NOAA (Figure S5). Only the results for nine regional climate divisions are shown here; results based on grid cells are presented in Figures S6, S8, and S9.

4.2.1. Impact of TCs

MERRA-2 reanalysis data are constrained by observations and include the synoptic conditions of observed TCs as represented at the model resolution of 0.625×0.5°. The frequencies of TCs per decade based on HURDAT2 and MERRA-2 from 1980 to 2015 are shown in Figure S1. The spatial distributions of TC occurrences are quite similar. The active seasons for TC are summer and fall, and the affected areas are mainly over the Southeast United States. The land-falling TCs affecting any grid cell in that area occur about once per decade in summer and fall. The frequencies of land-falling TC in the Atlantic are much higher than that in Pacific. The land-falling TCs from the Pacific only affect the western coastal areas of Mexico.

Although the frequencies of TC based on our detection criteria are underestimated over the tropics, likely due to MERRA-2 resolution, the general pattern over the land is closer to HURDAT2 than over the ocean. To estimate the impact of TC on drought demise, the following computations are based on observational HURDAT2 data, which provide the locations of TC centers. The affected areas of TCs are considered as all the grid cells within a 5-degree radius. Metrics *r1* and *r2*, defined in section 3.2.1, are

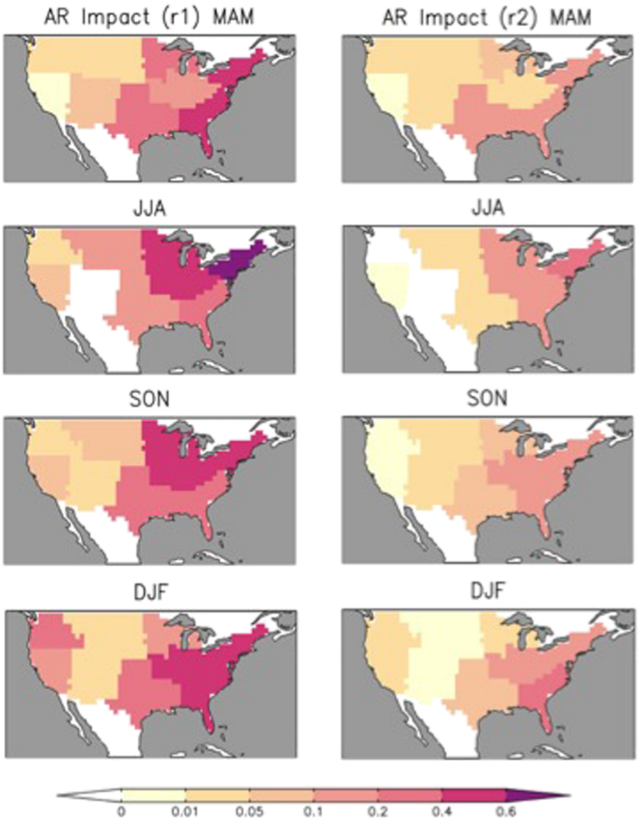

Figure 7. As in Figure 6 for atmospheric rivers (ARs).

calculated to estimate the impact of TC on meteorological drought demise.

The impacts of land-falling TCs on meteorological drought demise based on regional climate divisions are shown in Figure 6. TCs impact drought demise mainly during summer and winter in the Southeast, South, and central United States. In the Southeast United States, about 20–30% of the drought demise events are related to TC. Although TCs also occur in spring along the East Coast of the United States, they are not related to drought demise. The spottiness of grid cell based results in Figure S5 caused by the short time series of observational data is highly evident. Summer and fall are the preferred seasons of TC-related drought demise. About 20–40% of the drought demises are caused by land-falling TCs over the Southeast and Southern United States. There is a greater impact during fall further inland, over the southern, central, and southwestern United States.

The ratios that TC related SPI-6P change to the total SPI-6P deficit exceed 10% in the southeastern and central United States. The TC contribution in fall is mainly over the southern United States and southeastern United States. The TC-related precipitation contributing to drought demise in spring and winter is almost none.

4.2.2. Impact of ARs

Figure S7 displays the frequencies of AR occurrence in MERRA-2 over all seasons. The frequencies of ARs are substantially higher over the eastern United States than the western United States. In the eastern United States, there are more than 100 days with AR events per decade for each of the four seasons, and their orientation are more south-to-north than west-to-east (not shown). There is a pattern shift in the eastern United States from higher latitude to lower latitude from summer to winter. There are from 20 to 100 days with AR per decade along the West Coast of the United States in fall and winter and lower frequencies in spring and summer (not shown). There is an overestimation of AR frequency over the northern

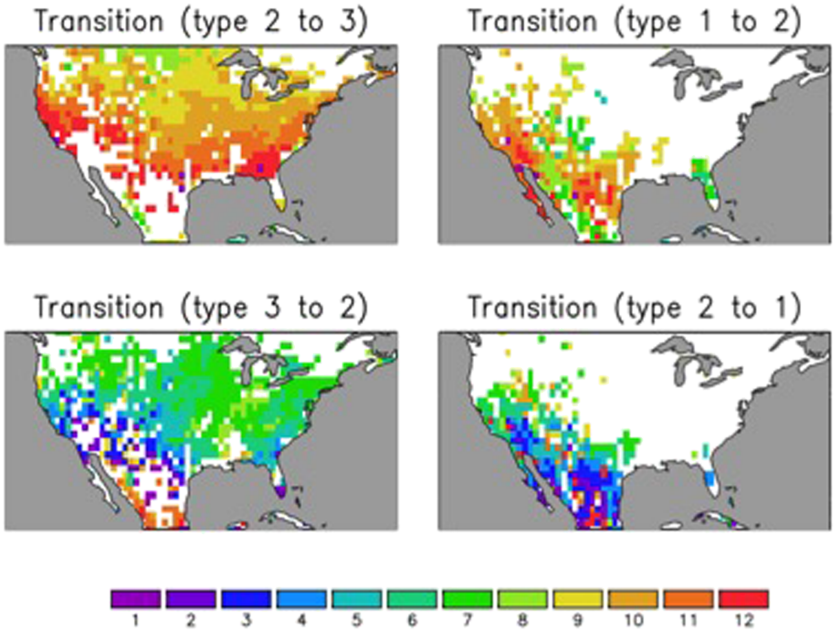

Figure 8. Mean transition month (1=January, 2=February, etc.) between regime types.

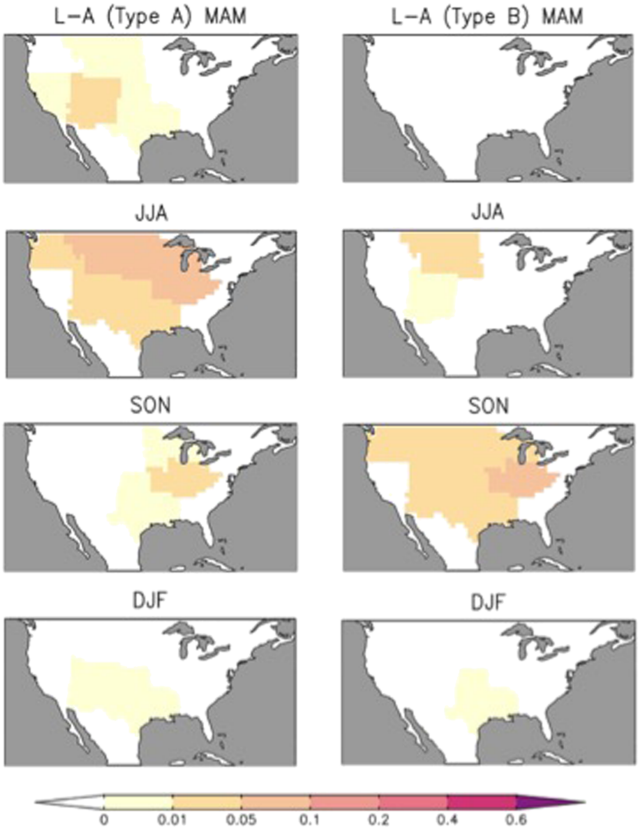

Figure 9. The fraction of drought demise related to Type A (left) and Type B (right) land atmospheric feedback changes.

United States. The algorithm was originally developed for the western United States during winter (Mundhenk et al., 2016), which may cause biases when applying it to other regions and seasons.

The impact of ARs on drought demise is also apparent in metrics r_1 and r_2. Figure 7 displays the ratios of AR impact on meteorological drought demise in MERRA-2. In the Northeast United States, more than 60% of the drought demises are related to AR. The impact decreases in fall and shifts to the southern United States in winter. The SPI-6P changes during the transition periods are also highly related to AR occurrences, which alleviate up to 40% of the SPI deficit over some parts of the northeastern United States and about 10–20% over the eastern and central United States (see Figure S8). The impact of ARs on drought demise over the western United States is not as significant as over the eastern United States. The major impact is on the Northwest coast in winter and along the southwestern coast. The patterns are rather noisy due to the relatively short period covered by MERRA-2.

4.3. Impact of LAF

The types of LAF transitions relate to drought demise are calculated based on MERRA-2 and are compared with the occurrence of drought demise. Figure 8 shows the months with LAF regime transitions. The seasonal transitions from Regimes 2 to 3, where soil moisture loses the ability to have positive feedback on surface fluxes to maintain drought, are generally from August to December, except over the Southwest United States. The transition is early in the northern United States and becomes later to the south. The transitions from regimes 3 to 2, where the atmosphere becomes sensitive to drier soils, are generally from May to August. This indicates that summer and fall are the periods with regime 2, which is related to type A LAF impact on drought demise, where dry soils can have a positive feedback on drought. The regime transition between types 1 and 2, between strong and transitional sensitivity, mainly occurs in the southwestern United States. The LAF regime transfers from types 1 to 2 in late fall and turn back to the hypersensitive type 1 in spring.

Figure 9 shows the fraction of drought demises related to LAF type A (increasing soil moisture from precipitation events) and type B (seasonal loss of sensitivity to soil moisture). Summer is the preferred season for type A impact on meteorological drought demise in MERRA-2. Up to 10% of the drought demises are related to type A over the central, east north central, and west north central United States in summer, and the impact is less in the other three seasons. Type B LAF occurs mainly in fall over the central United States and also over the northern United States in summer. The impact of Type B LAF is less frequent than the other causes that have been discussed.

4.4. Regional Summary

The figures in section 4 show clearly that there is a high degree of spatial variability among even adjacent grid cells. To ameliorate some of this noisiness in the results, the impacts of various causes of both meteorological drought demise in MERRA-2 are summarized by climate regions (defined in Figure S5) to identify the most important causes as well as the fraction of drought demises that are not explained by TC, AR, or LAF. Table 3 shows a summary of the dominant factors among those investigated for meteorological drought demise in MERRA-2 and the fractions of drought demise events that relate to the corresponding factors. Generally, AR is the most important factor for meteorological drought demise. AR accounts for about 20–25% of drought demise cases in United States. More than 30–40% of the meteorological drought demise events are related to AR in the Northeast United States, and the highest impact is found in summer, with about 62.7% of the events related to AR. In the Northwest United States, AR is identified as the most important factor for drought demise in fall and winter, but the ratios for AR-related drought demise are less than 10% except winter. The Southwest and Southeast U.S. regions

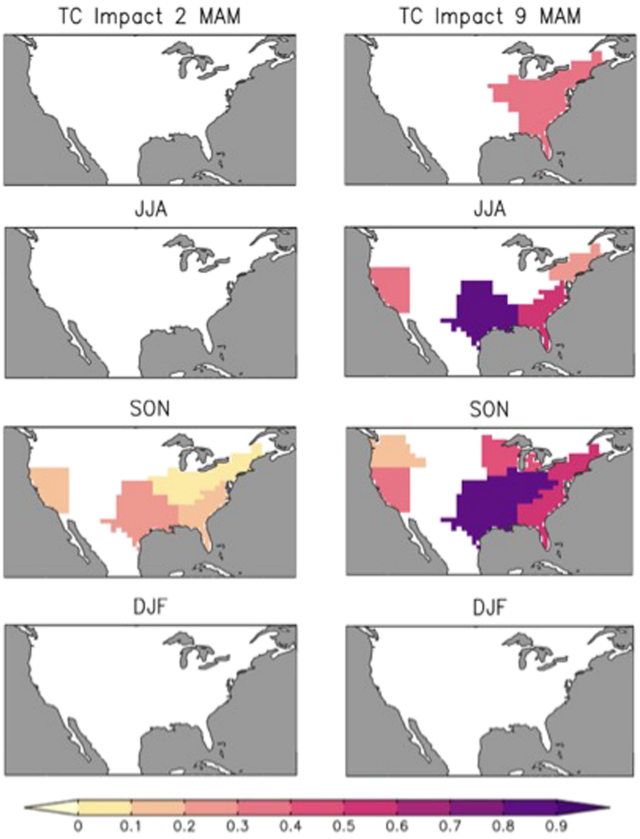

Figure 10. The fraction of comparisons showing the ratio (r1) of tropical cyclone (TC)-related drought demise based on selected short-term data (two ensemble members, left four panels; nine ensemble members, right four panels) is representative to the long-term data (absolute difference of ratios based on selected two ensemble members and all the ensemble members is lower than 0.05).

are impacted by TCs; therefore, TC is found to be the most significant cause for drought demise in fall. However, the ratio is high (30%) for the Southeast but low in the Southwest. No more than 10% of the drought demise events in this region are related to TC.

5. Representativeness

MERRA-2 data have been applied in the new framework of drought demise quantification and attributions. Reanalysis data are expected to represent real conditions. However, because the data length of MERRA-2 is less than 40 years, the results may not well represent the climatology of such extreme conditions and their attributions. Also, 30–40 years, while a common period for establishing weather climatologies, anomalies, and extremes, may not be sufficiently long to characterize the demise of extremes like drought. The representativeness test described in section 3 is applied using many centuries of climate model data from CESM-LE to determine how well the typical data length of observations or reanalysis reflects the characteristics of a long-term stationary climatology of the demise of an extreme event like drought. Analyses are repeated with data from CESM-LE spanning periods ranging from several decades, equivalent to MERRA-2, to over a century to see how well they represent the climatology of drought demise from nearly seven centuries of climate model data.

5.1. Representativeness of TC

The representativeness of the fraction of drought demise related to TC is tested first. Figure 10 shows the possibility that the ratio (r1) based on 32 years and 144 years data is representative to that of the long-term data set of 672 years from climate model data. Usually, 20–50% of the comparisons from the large Monte Carlo sample show that the results from 32 years data would be representative to the long-term frequency over the southeast and West United States, but the ratio is no more than 30% in fall. Figure S10 shows the representativeness based on each grid cell. From the results in Figures 10 and S10, 32 years, which is a common length for observed data and reanalysis data, is not long enough to represent locally the climatology of drought demise caused by TC. For the regional averages, the reliability increases because as the area increases the noise in the time series decreases relative to signal.

The comparison is repeated for lengths from 48 to 144 years, using 16-yearlong time series from more CESM-LE ensemble members. The probabilities that the ratios based on 144-year samples, shown in Figure 10, that are representative of the long-term climatology are much more prevalent than those for 32-year samples. Higher probability of representativeness is found over the Southeast United States and the West Coast in fall,

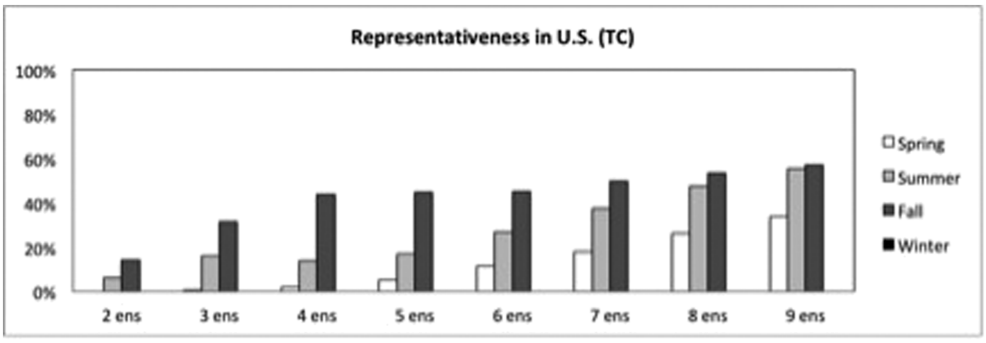

Figure 11. The averaged representativeness ratios in United States. The ratios indicate the percentages of tests showing representativeness in 10,000 tests for the ratios of tropical cyclone (TC)-related drought demise.

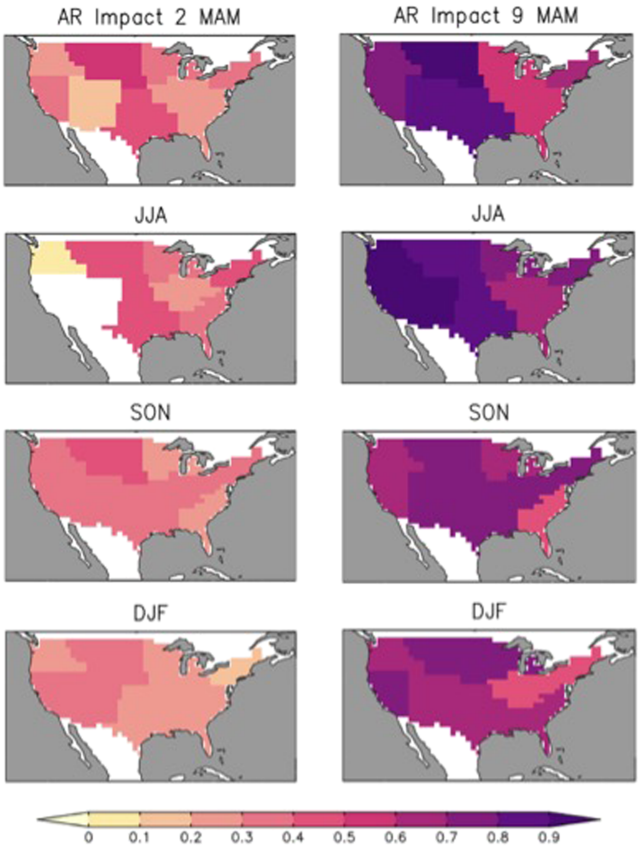

Figure 12. Same as Figure 10 for atmospheric river (AR).

because the frequencies of TC occurrences are naturally higher than the other seasons. The probabilities of representativeness reach 50–80% in the Southeast and along the West and South. Summer is another preferred season for TC occurrences; the probabilities of representativeness are about 50–80% in the Southeast and South and about 20–30% in the West. Compared with the local tests (Figure S10), the growing coherence and smoothness in the spatial extents of the shaded areas imply that the field significance for these regions is higher.

Figure 10 shows only two examples for sample sizes. To estimate how many years of data are needed to make the results statistically significant, bar charts for the representativeness for two to nine ensembles members spanning 32–144 years are plotted in Figure 11. The bar charts display the representativeness levels based on Monte Carlo tests. Based on CESM-LE, the most affected season is fall. With a common length for observational data (between two and three ensemble members for MERRA-2), the local probability of representativeness is no more than 30% in most of the TC affected areas. The low representativeness shown in Figure 11 relates to both the low rates of occurrence of TCs and of drought. The probabilities increase to more than 40% across when selecting four ensemble members (64 years) in fall. The representativeness also increases as sample size increases in spring and summer. No TC-related drought demise is found in winter; therefore, the representativeness test is not applied there.

5.2. Representativeness of AR

Figure 12 shows the fraction of tests shown to be representative for ARs when 32 and 144 years would constitute the observational record. The representativeness over the eastern United States is about 20–40% than in the western United States, except in summer. Because the ratios of AR-related drought demise are low over parts of the western United States in summer, the test of representativeness often fails to register results over much of the region then. In fall and winter, the probabilities of representativeness are 20% over Southeast United States. Higher representativeness (40–50%) is found over the central United States in winter. Generally, although the representativeness is higher for AR than TC, 32-year data are still not long enough to be locally representative of the long-term climatology.

The same assessment is repeated for 16-year intervals up to 144 years. As more ensemble members are added, the representativeness naturally increases. The right four panels in Figure 12 show the fraction of tests to be representative for AR with 144 years. The ratios showing representativeness are more than 50% over the United States for all the seasons. In spring and summer, the representativeness are higher than 60% in the northwestern, western, and central United States. Similar spatial distributions (higher representativeness in the West and lower in the East) are found in fall and winter. The local

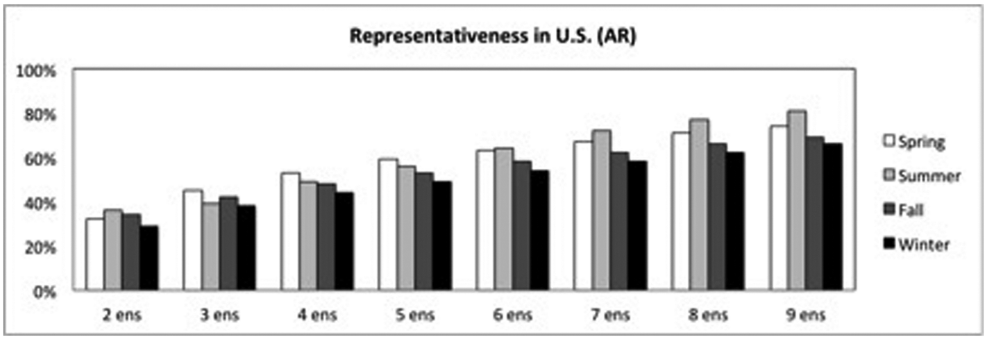

Figure 13. Same as Figure 11 for atmospheric river (AR).

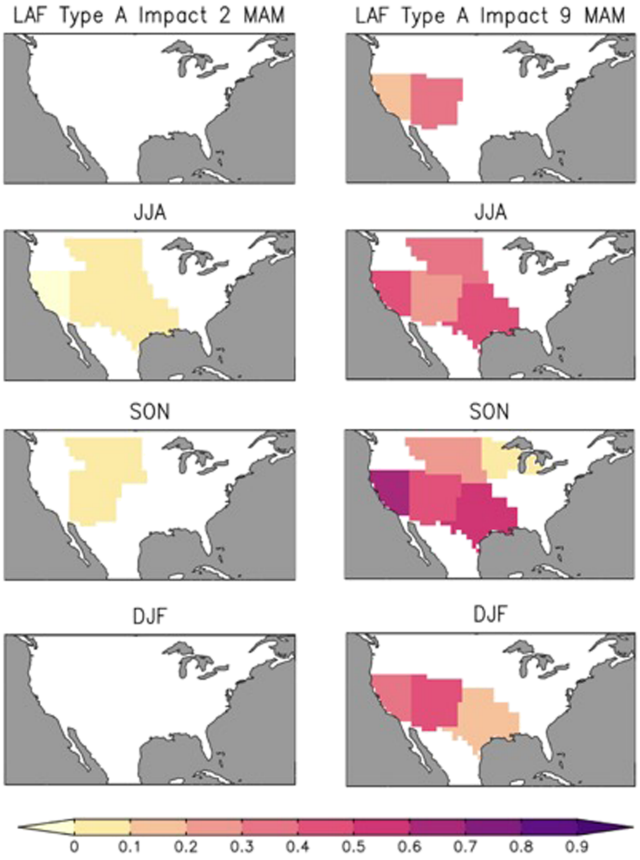

Figure 14. Same as Figure 10 for land atmospheric feedback (LAF).

representativeness of 144-year samples is still low over the western United States in summer and are related to the low ratios of AR-related drought demise in this region (Figure S11).

Figure 13 summarizes the results of average representativeness in United States for sample sizes from two to nine ensemble members (32–144 years). The change of average representativeness is quite similar in the four seasons. When taking two or three ensemble members (up to 48 years), the data generally have a probability of local representativeness higher than 40% in most of the regions. When selecting more ensemble members, the fractional areas show that the probability of the short-term data that is representative increases significantly. Seven to eight ensemble members (about 120 years) have a probability of representativeness more than 60%.

5.3. Representativeness of LAF

Figure 14 is the result of local representativeness tests for LAF with two and nine ensemble members. In this section, only the impact on drought demise of LAF type A (wetting of soil and desensitizing of surface fluxes to soil moisture content) is discussed. The ratio of LAF type B is low in all the grid points and seasons (lower than 0.05); therefore, the thresholds of representativeness (absolute differences lower than 0.05) are not enlightening for LAF type B. The probability that any two ensemble members (32 years) are representative of the long-term data is less than 10% for LAF type-A indicating that 32-year data are too short to be representative. The probabilities of representativeness increase to 20 to 50% with nine ensemble members over central and southwest United States. Although there is higher representativeness for 144 years than 32 years, the representativeness test can only be applied to 4–5 climate regional divisions due to lack of attribution events and the probabilities are much lower than AR and TC. As with TC and AR, compared with grid cell-based representativeness (Figure S12), regional coherence in LAF patterns suggests that in practical application, representativeness is somewhat greater than local tests suggest.

The bar chat in Figure 15 also shows low representativeness for LAF type A with different sample sizes. Type A LAF impacts are generally less frequent than TC or AR impacts. Therefore, the current data length is not long enough to represent the long-term local climatology for the impact of LAF type A on drought demise. Comparing Figure 14 to Figure 8, we see larger disagreement in spatial patterns between CESM-LE and MERRA-2 for LAF effects than for either TC or AR—thus, these representative results should taken even more cautiously. They point to the historic lack of validation and calibration of coupled land-atmosphere processes in weather and climate models (Santanello et al., 2018).

Since the data length of MERRA-2 is less than 48 years (three ensemble members), the representativeness test indicates that MERRA-2 likely cannot accurately represent the likelihood of each of the causes of drought

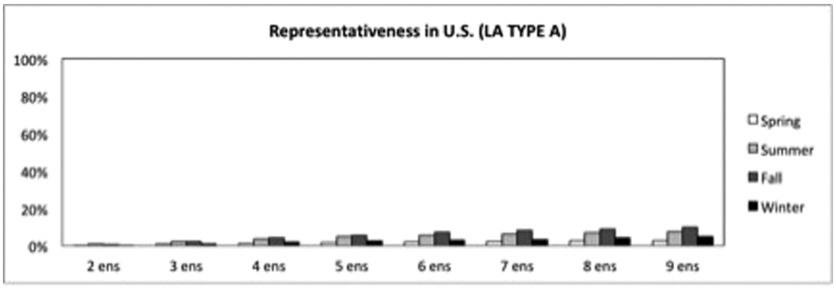

Figure 15. Same as Figure 11 for land atmospheric feedback (LAF) Type A.

demise at the local scale. To ensure that the results from MERRA-2 are statistically significant for the demise of extreme events like drought, a longer duration of data is required. An exchange of space for time increases robustness when drought demise attribution is considered on regional averages rather than local scales.

6. Discussion and Conclusions

This study has built a framework for the quantification and attribution of drought demise using MERRA-2 reanalysis data. We have defined a method to define the subseasonal transition period of meteorological drought demise based on SPI using pentad data rather than monthly. Using a higher temporal resolution data rather than monthly is to better capture the aspect that drought demise, which usually occurs much more quickly than drought onset and development. The preferred season for drought demise in MERRA-2 is spring over Southwest United States and summer over central and Northeast United States. We have also compared the patterns for drought onset and demise from MERRA-2 with the average of five observed precipitation data sets. There is a good agreement between them.

One of the novel contributions of this study is that we have quantified the transition period of drought demise. The transition period of drought demise has not been well studied compared to drought onset, even though the occurrence and speed of drought demise are just as important for social and economic interests. The transition period is well within subseasonal time scales, too short to be well captured by conventional techniques using monthly data. In this study, modified drought indices, SPI-6P for meteorological drought is developed to quantify drought at pentad (5-day) intervals. The average drought demise durations are about 3–7 pentads (15–35 days). Therefore, data with finer temporal resolution than monthly are recommended when quantifying drought demise. This short duration also lies well within the subseasonal time frame, which is potentially predictable (Robertson, Kumar, et al., 2015). One of the limitations of pentad-based data is that the results are noisier than monthly data and the durations of drought events may be underestimated.

Because of the short timescale for drought demise, it is a subseasonal prediction problem. Forecast skill for drought demise hinges on the ability to forecast its various causes. The attribution of TC, AR and LAF as factors in drought demise has been estimated for MERRA-2. TC-related drought demise accounts for about 30% of the total cases in summer and fall in the Southeast United States. The impacts are lower over the central United States and almost none in the West. AR frequency is higher than for TC over much of the United States and is higher over the eastern United States than the western United States. AR is the most important cause over the eastern United States, and it relates to more than 40% of the drought demise over Northeast United States. The contribution in the Northwest is lower, except in winter. The fraction of precipitation provided by AR to alleviate the total precipitation deficit is about 10–20% in the eastern United States. The impact of LAF type A is generally greatest in the central United States in summer and type B in fall. The impact of LAF is lower than the other two causes.

Inasmuch as MERRA-2 data are representative of the actual conditions over the United States, but with limited duration, the contributions to drought demise obtained from MERRA-2 data may not be able to represent the long-term climatological behavior of drought demise that might inform future behavior. A representativeness test is applied to different data lengths from 32 to 144 years on the contributions of TC, AR, and LAF on drought demise. The representativeness increases as the data length increases. Higher representativeness levels are shown with AR impact on drought demise than the other two causes. The purpose of representativeness testing is to identify if the MERRA-2 duration (36 years) is long enough to exemplify the local climatology of drought demise causes. The results show that by applying this method to observations, three decades of data (the traditional length for climatological benchmarks) likely is not be long enough to represent the inherent probabilities associated with all possible causes of drought demise. This issue is probably not unique to drought demise but is a problem for any extreme phenomena that lie in the tail of a probability distribution. However, the overall seasonality and the larger-scale regional patterns indicated in MERRA-2 are more representative of the likelihood of the drought demise causes investigated, as regional aggregation would ameliorate the problem of sample size to some extent.

By extending this framework, and with long enough data sets (Findell et al., 2014), we can get a general idea of how different causes impact drought demise in the United States and also provide guidance for drought mitigation, particularly at the regional scale. As AR and TC are considered as significant causes of drought demise over many regions, by well predicting their occurrence, we can better anticipate drought

termination, which is meaningful to agriculture and crop yields, especially for drought events during the growing season. For example, by considering the activities of the MJO and quasi-biennial oscillation, ARs can be predicted in 2–5 weeks in advance (Mundhenk et al., 2018). This early warning can provide guidance for farmers and decision makers over the regions where AR is an important cause of drought demise, as determined by this study.

Circulation regimes in the middle and high latitudes play a significant role in winter extreme events like floods over the United States (Robertson, Kushnir, et al., 2015). For example, Amini and Straus (2018) have identified circulation regimes based on 500-hPa geopotential height and 200-hPa zonal wind over the Pacific-North America region. Some of the impacts of the circulation regimes are included implicitly in the impact of ARs where the resulting moisture transport may affect preferred TC tracks. However, variations among circulation regimes may explain additional drought demise events not related to any of the three investigated causes over these areas, especially in winter.

Intraseasonal tropical climate variability, such as the phases of the Madden-Julian Oscillation (MJO), can also have a significant impact on the extreme events in the western United States (Bond & Vecchi, 2003). Summertime precipitation variability over the U.S. Great Plains may also be affected by the sea surface temperature changes in the tropical and northern Pacific and their associated teleconnections to North America (Ting & Wang, 1997). However, the effects of the MJO are felt locally through many of mechanisms described above, such as circulation changes, ARs, and even frequency of convection associated with MCSs. Fundamentally, these causes and those explicitly examined in this study are not unconnected, but TCs, ARs, and LAF are phenomenologically easier to isolate than remotely driven causes and thus have been the focus of this study. The interrelated nature of the climate system should not be forgotten in interpreting causes of drought demise, just as with drought onset, intensification, and maintenance. They all operate on subseasonal time scales.

Besides the causes discussed above, drought demise may also be triggered by internal atmospheric variability, which is essentially a random, unpredictable process on drought time scales that is not driven by detectable factors. For example, the sudden demise of drought in 2011 in Texas has been attributed to atmospheric chaos (Fernando et al., 2016). Studies also show that the internal atmospheric variability often contributes to winter extreme precipitation along the West Coast, which may account for as much as 80% of the total variance in precipitation (Lu et al., 2018). Although ARs and TCs are also part of internal variability, their impacts are much more significant to drought demise compared with others and are able to be quantified with model and reanalysis data. In this study, we separate these two from other elements of internal atmospheric variability because others are largely unpredictable on subseasonal to seasonal time scales. Therefore, if a drought demise is not related to any of the other possible mechanistic causes, it may be attributed by default to internal variability.

These additional potential causes may be added to the framework presented here in future studies. This point-by-point approach to assessing causes of drought demise may need to be aggregated in space to depict the demise of specific drought cases, just as the spatial scale of major droughts is composited from station, climate division, or grid cell data of local drought indices. Thus, this approach could be adapted to characterize the spatial as well as temporal evolution of drought demise, painting a more complete picture of the evolution of specific drought events. Finally, approaches to attributing these factors to the demise of agricultural drought can be performed using soil moisture data and the soil moisture deficit index (Narasimhan & Srinivasan, 2005) following the same approach—results are not shown here but they are quite similar to those based on SPI-6P (Wu, 2018). This framework could also be applied to hydrologic drought using streamflow data with further accounting of the different timescales in hydrographs among different size hydrologic units.

Acknowledgments
This research was supported by National Aeronautics and Space Administration grant NNX13AQ21G and by NOAA Climate Program Office from the Modeling, Analysis, Predictions, and Projections (MAPP) Program grant NA16OAR4310095. We acknowledge the CESM Large Ensemble Community Project and supercomputing resources provided by NCAR/CISL, supported from National Science Foundation grant AGS-1419445. We also acknowledge Brian Mundhenk at Colorado State University for providing us AR detection algorithm. We appreciate the useful discussion and help on this work provided by Liang Chen at George Mason University. The Modern-Era Retrospective Analysis for Research and Applications version 2 (MERRA-2) data are provided at http://goldsmr5.gesdisc.eosdis.nasa.gov/data/MERRA2/M2I3NVASM.5.12.4. GPCP One-Degree Daily (1DD) data Version 1.2 data are provided at www.daac.msfc.nasa.gov/pub/data/climatology . The CPC Unified Gauge-Based Analysis of precipitation data are provided at https://ftp.cpc.ncep.noaa.gov/precip/CPC_UNI_PRCP/GAUGE_CONUS/V1.0/. The Multi-Source Weighted-Ensemble Precipitation (MSWEP) data are provided at http://wald.anu.edu.au/data_services/data/mswep-multi-source-weighted-ensem%C2%ADble-pre%C2%ADcip%C2%ADi%C2%ADta%C2%ADtion/. Two versions of the Water and Global Change Forcing Data methodology applied to ERA-Interim data using the bias target Climatic Research Unit (WFDEI-CRU) and the German Weather Service Global Precipitation Climatology Centre WFDEI-GPCC are provided at https://rda.ucar.edu/datasets/ds314.2/. The Community Earth System Model, Large Ensemble Project data are provided from NCAR's Climate Data Gateway HPSS; please see: http://www.cesm.ucar.edu/projects/community-projects/LENS/ for details and means of data access. The North Atlantic Hurricane Database (HURDAT2) data are provided at https://www.nhc.noaa.gov/data/#hurdat.

References

Amini, S., & Straus, D. (2018). Control of storminess over the Pacific and North America by circulation regimes. The role of large-scale dynamics in weather extremes. *Climate Dynamics*, *54*, 4749–4770. https://doi.org/10.1007/s00382-018-4409-7

Barlow, M. (2011). Influence of hurricane-related activity on North American extreme precipitation. *Geophysical Research Letters*, *38*, L04705. https://doi.org/10.1029/2010GL046258

Beck, H. E., van Dijk, A. I. J. M., Levizzani, V., Schellekens, J., Miralles, D. G., Martens, B., & de Roo, A. (2017). MSWEP: 3-hourly 0.25° global gridded precipitation (1979–2015) by merging gauge, satellite, and reanalysis data. *Hydrology and Earth System Sciences*, *21*(1), 589–615. https://doi.org/10.5194/hess-21-589-2017

Bond, A. N., & Vecchi, A. G. (2003). The influence of the Madden–Julian oscillation on precipitation in Oregon and Washington. *Weather and Forecasting*, *18*(4), 600–613. https://doi.org/10.1175/1520-0434(2003)018<0600:TIOTMO>2.0.CO;2

Bonsal, B. R., Wheaton, E. E., Meinert, A., & Siemens, E. (2011). Characterizing the surface features of the 1999–2005 Canadian Prairie drought in relation to previous severe twentieth century events. *Atmosphere-Ocean*, *49*(4), 320–338. https://doi.org/10.1080/07055900.2011.594024

Brubaker, K. L., Dirmeyer, P. A., Sudradjat, A., Levy, B. S., & Bernal, F. (2001). A 36-yr climatological description of the evaporative sources of warm-season precipitation in the Mississippi River basin. *Journal of Hydrometeorology*, *2*(6), 537–557. https://doi.org/10.1175/1525-7541(2001)002<0537:AYCDOT>2.0.CO;2

Chapman, S. C., Stainforth, D. A., & Watkins, N. W. (2015). Limits to the quantification of local climate change. *Environmental Research Letters*, *10*, 094018. https://doi.org/10.1088/1748-9326/10/9/094018

Chen, M., Shi, W., Xie, P., Silva, V. B. S., Kousky, V. E., Wayne Higgins, R., & Janowiak, J. E. (2008). Assessing objective techniques for gauge-based analyses of global daily precipitation. *Journal of Geophysical Research*, *113*, D04110. https://doi.org/10.1029/2007JD009132

Christian, J., Basara, J., Otkin, J., Hunt, E., Wakefield, R., Flanagan, P., & Xiao, X. (2019). A methodology for flash drought identification: Application of flash drought frequency across the United States. *Journal of Hydrometeorology*, *20*(5), 833–846. https://doi.org/10.1175/JHM-D-18-0198.1

Clark, J. S., Grimm, E. C., Donovan, J. J., Fritz, S. C., Engstrom, D. R., & Almendinger, J. E. (2002). Drought cycles and landscape responses to past aridity on prairies of the Northern Great Plains, USA. *Ecology*, *83*(3), 595–601. https://doi.org/10.1890/0012-9658(2002)083[0595:DCALRT]2.0.CO;2

Cook, E. R., Kablack, M. A., & Jacoby, G. C. (1988). The 1986 drought in the southeastern United States: How rare an event was it? *Journal of Geophysical Research*, *93*(D11), 14,257–14,260. https://doi.org/10.1029/JD093iD11p14257

Crausbay, D. S., Ramirez, A. R., Carter, S. L., Cross, M. S., Hall, K. R., Bathke, D. J., et al. (2017). Defining ecological drought for the twenty-first century. *Bulletin of the American Meteorological Society*, *98*(12), 2543–2550. https://doi.org/10.1175/BAMS-D-16-0292.1

Dai, A. (2013). Increasing drought under global warming in observations and models. *Nature Climate Change*, *3*(1), 52–58. https://doi.org/10.1038/nclimate1633

Dettinger, M. D. (2013). Atmospheric rivers as drought busters on the US West Coast. *Journal of Hydrometeorology*, *14*(6), 1721–1732. https://doi.org/10.1175/JHM-D-13-02.1

Dirmeyer, A. P., Chen, L., Wu, J., Shin, C.-S., Huang, B., Cash, B. A., et al. (2018). Verification of land–atmosphere coupling in forecast models, reanalyses, and land surface models using flux site observations. *Journal of Hydrometeorology*, *19*(2), 375–392. https://doi.org/10.1175/JHM-D-17-0152.1

Dirmeyer, A. P., Schlosser, C. A., & Kaye, L. B. (2009). Precipitation, recycling, and land memory: An integrated analysis. *Journal of Hydrometeorology*, *10*(1), 278–288. https://doi.org/10.1175/2008JHM1016.1

Dirmeyer, P. A., & Brubaker, K. L. (1999). Contrasting evaporative moisture sources during the drought of 1988 and the flood of 1993. *Journal of Geophysical Research*, *104*(D16), 19,383–19,397. https://doi.org/10.1029/1999JD900222

Dirmeyer, P. A., & Kinter, J. L. (2009). The "Maya Express": Floods in the U.S. Midwest. *Eos, Transactions American Geophysical Union*, *90*(12), 101–102. https://doi.org/10.1029/2009EO120001

Dracup, J. A., Lee, K. S., & Paulson, E. G. (1980). On the definition of droughts. *Water Resources Research*, *16*(2), 297–302. https://doi.org/10.1029/WR016i002p00297

Durre, I., John, M. W., & Dennis, P. L. (2000). Dependence of Extreme Daily Maximum Temperatures on Antecedent Soil Moisture in the Contiguous United States during Summer. *Journal of Climate*, *13*(14), 2641–2651. https://doi.org/10.1175/1520-0442(2000)013<2641:DOEDMT>2.0.CO;2

Eltahir, E. A. B. (1998). A soil moisture–rainfall feedback mechanism: 1. Theory and observations. *Water Resources Research*, *34*(4), 765–776. https://doi.org/10.1029/97WR03499

Fernando, D. N., Mo, K. C., Fu, R., Bowerman, A. R., Scanlon, B. R., Solis, R., et al. (2016). What caused the spring intensification and winter demise of the 2011 drought over Texas? *Climate Dynamics*, *47*(9-10), 3077–3090. https://doi.org/10.1007/s00382-016-3014-x

Fierro, O. A., Robert, F. R., Frank, D. M., & David, S. N. (2009). The impact of horizontal grid spacing on the microphysical and kinematic structures of strong tropical cyclones simulated with the WRF-ARW model. *Monthly Weather Review*, *137*(11), 3717–3743. https://doi.org/10.1175/2009MWR2946.1

Findell, K. L., & Eltahir, E. A. B. (2003). Atmospheric Controls on soil moisture–boundary layer interactions. Part I: Framework development. *Journal of Hydrometeorology*, *4*(3), 552–569. https://doi.org/10.1175/1525-7541(2003)004<0552:ACOSML>2.0.CO;2

Findell, K. L., Gentine, P., Lintner, B. R., & Guillod, B. P. (2014). Data length requirements for observational estimates of land–atmosphere coupling strength. *Journal of Hydrometeorology $V*, *16*(4), 1615–1635. https://doi.org/10.1175/JHM-D-14-0131.1

Fischer, E. M., Seneviratne, S. I., Lüthi, D., & Schär, C. (2007). Contribution of land-atmosphere coupling to recent European summer heat waves. *Geophysical Research Letters*, *34*, L06707. https://doi.org/10.1029/2006GL029068

Gelaro, R., McCarty, W., Suárez, M. J., Todling, R., Molod, A., Takacs, L., et al. (2017). The Modern-Era Retrospective Analysis for Research and Applications, Version 2 (MERRA-2). *Journal of Climate*, *30*(14), 5419–5454. https://doi.org/10.1175/JCLI-D-16-0758.1

Gommes, R. A., and F. Petrassi (1994), Rainfall Variability and Drought in Sub-Saharan Africa Since 1960, FAO, Research and Technology Development Division, Agrometeorology Group.

Haghighi, E., Short Gianotti, D. J., Akbar, R., Salvucci, G. D., & Entekhabi, D. (2018). Soil and atmospheric controls on the landsurface energy balance: A generalized framework for distinguishing moisture-limited and energy-limited evaporation regimes. *Water Resources Research*, *54*, 1831–1851. https://doi.org/10.1002/2017WR021729

Hao, Z., Singh Vijay, P., & Xia, Y. (2018). Seasonal drought prediction: Advances, challenges, and future prospects. *Reviews of Geophysics*, *56*(1), 108–141. https://doi.org/10.1002/2016RG000549

Harding, R., Best, M., Blyth, E., Hagemann, S., Kabat, P., Tallaksen, L. M., et al. (2011). WATCH: Current knowledge of the terrestrial global water cycle. *Journal of Hydrometeorology*, *12*(6), 1149–1156. https://doi.org/10.1175/JHM-D-11-024.1

Harris, I., Jones, P. D., Osborn, T. J., & Lister, D. H. (2014). Updated high-resolution grids of monthly climatic observations—The CRU TS3.10 Dataset. *International Journal of Climatology*, *34*(3), 623–642. https://doi.org/10.1002/joc.3711

Heim, R. R. Jr. (2002). A review of twentieth-century drought indices used in the United States. *Bulletin of the American Meteorological Society*, *83*(8), 1149–1166. https://doi.org/10.1175/1520-0477-83.8.1149

Hoerling, M., & Kumar, A. (2003). The perfect ocean for drought. *Science*, *299*(5607), 691–694. https://doi.org/10.1126/science.1079053

Huffman, J. G., Robert, F. A., Mark, M. M., David, T. B., Scott, C., Robert, J., et al. (2001). Global precipitation at one-degree daily resolution from multisatellite observations. *Journal of Hydrometeorology*, *2*(1), 36–50. https://doi.org/10.1175/1525-7541(2001)002<0036:GPAODD>2.0.CO;2

Hurrell, W. J., Holland, M. M., Gent, P. R., Ghan, S., Kay, J. E., Kushner, P. J., et al. (2013). The Community Earth System Model: A framework for collaborative research. *Bulletin of the American Meteorological Society*, *94*(9), 1339–1360. https://doi.org/10.1175/BAMS-D-12-00121.1

Kam, J., Justin, S., Xing, Y., & Eric, F. W. (2013). The influence of Atlantic Tropical cyclones on drought over the Eastern United States (1980–2007). *Journal of Climate*, *26*(10), 3067–3086. https://doi.org/10.1175/JCLI-D-12-00244.1

Kay, J. E., Deser, C., Phillips, A., Mai, A., Hannay, C., Strand, G., et al. (2015). The Community Earth System Model (CESM) Large Ensemble Project: A community resource for studying climate change in the presence of internal climate variability. *Bulletin of the American Meteorological Society*, *96*(8), 1333–1349. https://doi.org/10.1175/BAMS-D-13-00255.1

Knight, D. B., & Davis, R. E. (2007). Climatology of tropical cyclone rainfall in the Southeastern United States. *Physical Geography*, *28*(2), 126–147. https://doi.org/10.2747/0272-3646.28.2.126

Koster, R. D., Schubert, S. D., & Suarez, M. J. (2009). Analyzing the concurrence of meteorological droughts and warm periods, with implications for the determination of evaporative regime. *Journal of Climate*, *22*(12), 3331–3341. https://doi.org/10.1175/2008JCLI2718.1

Lam, H., Kok, M. H., & Shum, K. K. Y. (2012). Benefits from typhoons—The Hong Kong perspective. *Weather*, *67*(1), 16–21. https://doi.org/10.1002/wea.836

Landsea, C., & Franklin, J. (2013). Atlantic hurricane database uncertainty and presentation of a new database format. *Monthly Weather Review*, *141*(10), 3576–3592. https://doi.org/10.1175/MWR-D-12-00254.1

Lawrence, D. M., Oleson, K. W., Flanner, M. G., Thornton, P. E., Swenson, S. C., Lawrence, P. J., et al. (2011), Parameterization improvements and functional and structural advances in Version 4 of the Community Land Model, *Journal of Advances in Modeling Earth Systems*, *3*, M03001, https://doi.org/10.1029/2011MS00045

Lu, D., Leung, L. R., Fengfei, S., & Jian, L. (2018). Roles of SST versus internal atmospheric variability in winter extreme precipitation variability along the U.S. West Coast. *Journal of Climate*, *31*(19), 8039–8058. http://doi.org/10.1175/JCLI-D-18-0062.1

Manganello, V. J., Hodges, K. I., Kinter, J. L. III, Cash, B. A., Marx, L., Jung, T., et al. (2012). Tropical cyclone climatology in a 10-km global atmospheric GCM: Toward weather-resolving climate modeling. *Journal of Climate*, *25*(11), 3867–3893. https://doi.org/10.1175/JCLI-D-11-00346.1

Margulis, S. A., Cortés, G., Girotto, M., Huning, L. S., Li, D., & Durand, M. (2016). Characterizing the extreme 2015 snowpack deficit in the Sierra Nevada (USA) and the implications for drought recovery. *Geophysical Research Letters*, *43*, 6341–6349. https://doi.org/10.1002/2016GL068520

Marsh, T. (2007). The 2004–2006 drought in southern Britain. *Weather*, *62*(7), 191–196. https://doi.org/10.1002/wea.99

Maxwell, J., Soulé, P. T., Ortegren, J. T., & Knapp, P. A. (2012). Drought- busting tropical cyclones in the Southeastern Atlantic United States: 1950–2008. *Annals of the Association of American Geographers*, *102*(2), 259–275. https://doi.org/10.1080/00045608.2011.596377

Maxwell, J. T., Knapp, P. A., Ortegren, J. T., Ficklin, D. L., & Soulé, P. T. (2017). Changes in the mechanisms causing rapid drought cessation in the Southeastern United States of America. *Geophysical Research Letters*, *44*, 12,476–12,483. https://doi.org/10.1002/2017GL076261

Maxwell, T. J., Jason, T. O., Paul, A. K., & Peter, T. S. (2013). Tropical cyclones and drought amelioration in the Gulf and Southeastern Coastal United States. *Journal of Climate*, *26*(21), 8440–8452. https://doi.org/10.1175/JCLI-D-12-00824.1

McKee, T. B., N. J. Doesken, and J. Kleist (1993), The relationship of drought frequency and duration to time scales, paper presented at Proceedings of the 8th Conference on Applied Climatology, American Meteorological Society Boston, MA, USA.

Mishra, A. K., & Singh, V. P. (2010). A review of drought concepts. *Journal of Hydrology*, *391*(1–2), 202–216. https://doi.org/10.1016/j.jhydrol.2010.07.012

Misra, V., & Bastola, S. (2016). Reconciling droughts and landfalling tropical cyclones in the Southeastern United States. *Climate Dynamics*, *46*(3-4), 1277–1286. https://doi.org/10.1007/s00382-015-2645-7

Mo, K. C. (2011). Drought onset and recovery over the United States. *Journal of Geophysical Research*, *116*, D20106. https://doi.org/10.1029/2011JD016168

Molod, A., Takacs, L., Suarez, M., & Bacmeister, J. (2015). Development of the GEOS-5 atmospheric general circulation model: evolution from MERRA to MERRA2. *Geoscientific Model Development*, *8*(5), 1339–1356. https://doi.org/10.5194/gmd-8-1339-2015

Mueller, B., & Seneviratne, S. I. (2012). Hot days induced by precipitation deficits at the global scale. *Proceedings of the National Academy of Sciences*, *109*(31), 12,398–12,403. https://doi.org/10.1073/pnas.1204330109

Muggeo, V. M. (2003). Estimating regression models with unknown break-points. *Statistics in Medicine*, *22*(19), 3055–3071. https://doi.org/10.1002/sim.1545

Muggeo, V. M. R. (2008), Segmented: An R package to fit regression models with broken-line relationships, paper presented at R News.

Mundhenk, B. D., Barnes, E. A., Maloney, E. D., & Baggett, C. F. (2018). Skillful empirical subseasonal prediction of landfalling atmospheric river activity using the Madden–Julian oscillation and quasi-biennial oscillation. *NPJ Climate and Atmospheric Science*, *1*, 20177. https://doi.org/10.1038/s41612-017-0008-2

Mundhenk, B. D., Elizabeth, A. B., & Eric, D. M. (2016). All-season climatology and variability of atmospheric river frequencies over the North Pacific. *Journal of Climate*, *29*(13), 4885–4903. https://doi.org/10.1175/JCLI-D-15-0655.1

Narasimhan, B., & Srinivasan, R. (2005). Development and evaluation of Soil Moisture Deficit Index (SMDI) and Evapotranspiration Deficit Index (ETDI) for agricultural drought monitoring. *Agricultural and Forest Meteorology*, *133*(1–4), 69–88. https://doi.org/10.1016/j.agrformet.2005.07.012

NIDIS (2018), 2017's Billion-Dollar Disasters, edited.

Otkin, A. J., Yafang, Z., Eric, D. H., Jeff, B., Mark, S., Martha, C. A., & Christopher, H. (2019). Assessing the evolution of soil moisture and vegetation conditions during a flash drought–flash recovery sequence over the South-Central United States. *Journal of Hydrometeorology*, *20*(3), 549–562. https://doi.org/10.1175/JHM-D-18-0171.1

Parry, S., Prudhomme, C., Wilby, R. L., & Wood, P. J. (2016). Drought termination: Concept and characterisation. *Progress in Physical Geography*, *40*(6), 743–767. https://doi.org/10.1177/0309133316652801

Pu, B., Fu, R., Dickinson, R. E., & Fernando, D. N. (2016). Why do summer droughts in the Southern Great Plains occur in some La Niña years but not others? *Journal of Geophysical Research: Atmospheres*, *121*, 1120–1137. https://doi.org/10.1002/2015JD023508

Ralph, F., & Dettinger, M. (2012). Historical and national perspectives on extreme West Coast precipitation associated with atmospheric rivers during December 2010. *Bulletin of the American Meteorological Society*, *93*(6), 783–790. https://doi.org/10.1175/BAMS-D-11-00188.1

Ralph, F. M., Michael, D. D., Mary, M. C., Thomas, J. G., & John, E. (2018). Defining "atmospheric river": How the glossary of meteorology helped resolve a debate. *Bulletin of the American Meteorological Society*, *99*(4), 837–839. https://doi.org/10.1175/BAMS-D-17-0157.1

Reichle, H. R., Liu, Q., Randal, D. K., Clara, S. D., Sarith, P. P. M., & Gary, S. P. (2017). Land surface precipitation in MERRA-2. *Journal of Climate*, *30*(5), 1643–1664. https://doi.org/10.1175/JCLI-D-16-0570.1

Rippey, B. R. (2015). The U.S. drought of 2012. *Weather and Climate Extremes*, *10*, 57–64. https://doi.org/10.1016/j.wace.2015.10.004

Robertson, A. W., Kumar, A., Peña, M., & Vitart, F. (2015). Improving and promoting subseasonal to seasonal prediction. *Bulletin of the American Meteorological Society*, *96*(3), ES49–ES53. https://doi.org/10.1175/BAMS-D-14-00139.1

Robertson, A. W., Y. Kushnir, Lall, U., and J. Nakamura (2015), Weather and climatic drivers of extreme flooding events over the Midwest of the United States.

Ronald, G., McCarty, W., Suárez, M. J., Todling, R., Molod, A., Takacs, L., et al. (2017). The Modern-Era Retrospective Analysis for Research and Applications, Version 2 (MERRA-2). *Journal of Climate*, *30*(14), 5419–5454. https://doi.org/10.1175/JCLI-D-16-0758.1

Roundy, J. K., Ferguson, C. R., & Wood, E. F. (2013). Temporal Variability of land-atmosphere coupling and its implications for drought over the Southeast United States. *Journal of Hydrometeorology*, *14*(2), 622–635. https://doi.org/10.1175/JHM-D-12-090.1

Rutz, J. J., & Steenburgh, W. J. (2012). Quantifying the role of atmospheric rivers in the interior western United States. *Atmospheric Science Letters*, *13*(4), 257–261. https://doi.org/10.1002/asl.392

Santanello, A. J., Dirmeyer, P. A., Ferguson, C. R., Findell, K. L., Tawfik, A. B., Berg, A., et al. (2018). Land–atmosphere interactions: The LoCo perspective. *Bulletin of the American Meteorological Society*, *99*(6), 1253–1272. https://doi.org/10.1175/BAMS-D-17-0001.1

Schubert, S., Gutzler, D., Wang, H., Dai, A., Delworth, T., Deser, C., et al. (2009). A U.S. CLIVAR project to assess and compare the responses of global climate models to drought-related SST forcing patterns: Overview and results. *Journal of Climate*, *22*(19), 5251–5272. https://doi.org/10.1175/2009JCLI3060.1

Seager, R., Alexandrina, T., & Jennifer, N. (2009). Drought in the Southeastern United States: Causes, variability over the last millennium, and the potential for future hydroclimate change. *Journal of Climate*, *22*(19), 5021–5045. https://doi.org/10.1175/2009JCLI2683.1

Seager, R., Goddard, L., Nakamura, J., Henderson, N., & Lee, D. E. (2014). Dynamical causes of the 2010/11 Texas-Northern Mexico drought. *Journal of Hydrometeorology*, *15*(1), 39–68. https://doi.org/10.1175/JHM-D-13-024.1

Seneviratne, S. I., Koster, R. D., Guo, Z., Dirmeyer, P. A., Kowalczyk, E., Lawrence, D., et al. (2006). Soil moisture memory in AGCM simulations: Analysis of Global Land–Atmosphere Coupling Experiment (GLACE) data. *Journal of Hydrometeorology*, *7*(5), 1090–1112. https://doi.org/10.1175/JHM533.1

Sun, Y., Fu, R., Dickinson, R., Joiner, J., Frankenberg, C., Gu, L., et al. (2015). Drought onset mechanisms revealed by satellite solar-induced chlorophyll fluorescence: Insights from two contrasting extreme events. *Journal of Geophysical Research: Biogeosciences*, *120*, 2427–2440. https://doi.org/10.1002/2015JG003150

Susskind, J., Piraino, P., Rokke, L., Iredell, L., & Mehta, A. (1997). Characteristics of the TOVS Pathfinder Path A dataset. *Bulletin of the American Meteorological Society*, *78*(7), 1449–1472. https://doi.org/10.1175/1520-0477(1997)078<1449:COTTPP>2.0.CO;2

Tawfik, A. B., & Dirmeyer, P. A. (2014). A process-based framework for quantifying the atmospheric preconditioning of surface-triggered convection. *Geophysical Research Letters*, *41*, 173–178. https://doi.org/10.1002/2013GL057984

Ting, M., & Wang, H. (1997). Summertime U.S. precipitation variability and its relation toPacific Sea Surface Temperature. *Journal of Climate*, *10*(8), 1853–1873. https://doi.org/10.1175/1520-0442(1997)010<1853:SUSPVA>2.0.CO;2

Walsh, K. J. E., Fiorino, M., Landsea, C. W., & McInnes, K. L. (2007). Objectively determined resolution-dependent threshold criteria for the detection of tropical cyclones in climate models and reanalyses. *Journal of Climate*, *20*(10), 2307–2314. https://doi.org/10.1175/JCLI4074.1

Weedon, G. P., Balsamo, G., Bellouin, N., Gomes, S., Best, M. J., & Viterbo, P. (2014). The WFDEI meteorological forcing data set: WATCH Forcing Data methodology applied to ERA-Interim reanalysis data. *Water Resources Research*, *50*, 7505–7514. https://doi.org/10.1002/2014WR015638

Wilhite, D. A., & Glantz, M. H. (1985). Understanding: the drought phenomenon: The role of definitions. *Water International*, *10*(3), 111–120. https://doi.org/10.1080/02508068508686328

Wood, E. F., Schubert, S. D., Wood, A. W., Peters-Lidard, C. D., Mo, K. C., Mariotti, A., & Pulwarty, R. S. (2015). Prospects for advancing drought understanding, monitoring, and prediction. *Journal of Hydrometeorology*, *16*(4), 1636–1657. https://doi.org/10.1175/JHM-D-14-0164.1

Wu, J. (2018), Drought demise quantification and attribution over CONUS, George Mason University.

Xie, J., & Zhang, M. (2017). Role of internal atmospheric variability in the 2015 extreme winter climate over the North American continent. *Geophysical Research Letters*, *44*, 2464–2471. https://doi.org/10.1002/2017GL072772